EFFECT OF LARGE-AMPLITUDE PERPENDICULARLY-PROPAGATING RF WAVES ON THE INTERCHANGE INSTABILITY

by

Neils F. Otani and Bruce I. Cohen

Memorandum No. UCB/ERL M86/48

8 July 1986

EFFECT OF LARGE-AMPLITUDE PERPENDICULARLY-PROPAGATING RF WAVES ON THE INTERCHANGE INSTABILITY

by

Neils F. Otani and Bruce I. Cohen

Memorandum No. UCB/ERL M86/48

8 July 1986

ELECTRONICS RESEARCH LABORATORY

College of Engineering
University of California, Berkeley
94720

EFFECT OF LARGE-AMPLITUDE PERPENDICULARLY-PROPAGATING RF WAVES ON THE INTERCHANGE INSTABILITY

by

Neils F. Otani and Bruce I. Cohen

Memorandum No. UCB/ERL M86/48

8 July 1986

ELECTRONICS RESEARCH LABORATORY

College of Engineering
University of California, Berkeley
94720

Effect of Large-Amplitude Perpendicularly-Propagating RF Waves on the Interchange Instability

Niels F. Otani*
Electronics Research Laboratory
University of California
Berkeley, California 94720

Bruce I. Cohen
Lawrence Livermore National Laboratory
University of California
Livermore, California 94550

Results are presented from hybrid 2-d quasineutral Darwin simulations of the interchange instability in the presence of a large RF wave in the ion-cyclotron frequency range. The simulation models the plane perpendicular to the background magnetic field using cold, particle ions and a cold $\mathbf{E} \times \mathbf{B}$ electron fluid. Related theory is also discussed. Fluid equations appropriate to our simulation model are derived and their properties demonstrated and compared to simulation. A method for solving for the RF-modified growth rates from the fluid equations is described. It is generally expected that the current component associated with the mean, RF-induced ion drift is capable of influencing the stability of the interchange mode; however, no modification of the mean ion drift is observed in simulations in which RF is present. Instead, in both the theory and simulation, an electron RF-field oscillation current dominates the modification to the gravitational current. As a result, even in the presence of large RF fields, ($B_{RF}/B_0 = 15\%$) only modest corrections to the interchange growth rates are observed. The effect is stabilizing for $kL_n \lesssim 0.8$–0.9, apparently for both signs of the square-electric-field gradient, and is destabilizing for larger values of kL_n, although the credibility of the simulation begins to become suspect here. Fractional reduction of the interchange growth rate is observed to be quadratically dependent on the RF wave amplitude, independent of ion-cyclotron resonant effects, and proportional to $\nabla B_{RF}^2/\nabla B_0^2$, consistent with an eikonal theory developed for the study of stabilizing effects on perpendicularly-propagating fast Alfvén waves. The results also suggest that additional gradient-independent stabilizing effects may be operative when $kL_n \sim 1$. Finally, it is also observed that, while the RF wave has little effect on the interchange instability, the interchange mode strongly affects the RF wave, damping it significantly as the mode saturates.

* Present address: Courant Institute of Mathematical Sciences, New York University, New York, New York 10012.

I. INTRODUCTION

Recent results from the Phaedrus tandem mirror experiment at Wisconsin [1] have stimulated much interest in the possibility of stabilizing the interchange modes in axisymmetric mirror devices by means of an applied RF field in the ion-cyclotron frequency range. It was observed in the Phaedrus experiment that a small decrease ($\sim 0.4\%$) in the static mirror magnetic field strength produced a dramatic change in measured plasma density fluctuations. Since the fixed frequency of the RF field, ω_0, was very close to the ion-cyclotron frequency, ω_{ci}, when these measurements were taken, it was concluded that the stabilizing effect indicated by the reduction in the density fluctuations was occurring when the frequency of the RF field was greater than, but not when the frequency was less than, the ion-cyclotron frequency. Further, it was suggested that the stabilizing agent was a ponderomotive force associated with the radial gradient in the applied RF field. One could then speculate that such a force would counter the effective radial gravity driving the interchange instability. The abrupt onset of stability is also then explained since, in its simplest form, the force may be expressed as [2]

$$\mathbf{F}_p = -\frac{e^2}{4m}\frac{\nabla|E_1|^2}{\omega_0^2 - \omega_{ci}^2}, \tag{1}$$

which changes sign and is largest as the ion-cyclotron resonance is crossed. Here m is the ion mass and E_1 is the magnitude of the RF wave electric field.

Unfortunately, this intuitively appealing physical picture has not been borne out either by other experiments or by theoretical studies. Earlier measurements taken on the HX-II at Kyoto [3] provide evidence that the stabilizing effect of RF on a related $\mathbf{E} \times \mathbf{B}$ rotation-induced instability is strongest near the ion cyclotron frequency, but stability is observed on *both* sides of the resonance. Suppression of flute oscillations has also been observed in the HIEI machine at Kyoto [4] in the presence of RF, at frequencies above the second ion cyclotron harmonic.

On the theoretical front, it seems likely that the ponderomotive force does play a role in the stabilization process. It seems equally likely however that the process cannot be explained in terms of a simple balance between the ponderomotive force and an effective gravity. Instead, a number of effects probably contribute.

Just as the behavior of a magnetized plasma as a whole is at least in theory completely described by the motion of its magnetized particles, so might one expect that the modification of particle orbits by a strong RF wave would lead to a fundamental understanding of plasma stability properties in the presence of RF. At first sight, the analysis seems almost trivial: for an electrostatic wave, the ponderomotive force term appears as a square

first-order term ($\langle \mathbf{x}_1 \cdot \nabla \mathbf{E}_1 \rangle$) when the ion Newton-Lorentz equation is expanded to second order in the RF wave amplitude and averaged over the ω_0^{-1}-timescale:

$$\left\langle \frac{d\mathbf{v}_2}{dt} \right\rangle = \frac{e}{m} \langle \mathbf{x}_1 \cdot \nabla \mathbf{E}_1(\mathbf{x}_0) \rangle + \frac{e}{mc} \langle \mathbf{v}_2 \rangle \times \mathbf{B}_0. \tag{2}$$

Substitution of linear expressions obtained from the first order Newton-Lorentz equation for the first-order quantities in this term leads immediately to Eq. (1).

There are, however, other complicating effects. In early stability treatments by Kishimoto [5] and Yamamoto [6], the RF wave was allowed to be electromagnetic, and modifications to stability due to the nonlinear term $\mathbf{v}_1 \times \mathbf{B}_1$ were considered. In Yamamoto's study, the presence of RF was stabilizing for ω_0 above ω_{ci} and destabilizing for ω_0 below ω_{ci}, as was observed in Phaedrus. Neither treatment is likely to be applicable to Phaedrus however, since the electrostatic component of the RF wave was ignored, so the longitudinal ponderomotive force term of the form $\langle x_1 \partial E_{x1}/\partial x \rangle$ was not included.

Another single particle effect of importance has been studied by Dimonte, Lamb, and Morales [2,7,8] in a series of papers concerned with the removal of the $\omega_0 = \omega_{ci}$ singularity in Eq. (1). It was demonstrated both experimentally and theoretically that the finite length of time a particle spends in the RF field due to the field's finite axial extent and the particle's nonzero axial velocity leads to a resolution of the singularity. The ponderomotive force is found to be finite for all values of the RF frequency in the vicinity of ω_{ci}, and in fact the peak ponderomotive force is found to occur when ω_0 is somewhat removed from ω_{ci}.

Further complications are encountered when a fluid model of the stabilizing mechanism is examined. As noted by several researchers, expressions obtained for the ponderomotive force from fluid theory differ in form and seemingly in essence from those obtained from single particle theory. When the ponderomotive $\langle \mathbf{u}_1 \cdot \nabla \mathbf{u}_1 \rangle$ term of the fast-timescale-averaged fluid ion momentum equation,

$$\left\langle \frac{\partial \mathbf{u}_2}{\partial t} \right\rangle = - \langle \mathbf{u}_1 \cdot \nabla \mathbf{u}_1 \rangle + \frac{e}{mc} \langle \mathbf{u}_2 \rangle \times \mathbf{B}_0, \tag{3}$$

is evaluated, the ponderomotive force is found to be

$$-m \langle \mathbf{u}_1 \cdot \nabla \mathbf{u}_1 \rangle = -\frac{e^2}{4m} \frac{\omega_0^2}{(\omega_0^2 - \omega_{ci}^2)^2} \nabla |E_1|^2, \tag{4}$$

which is not only different from Eq. (1), but also does *not* change sign across the resonance. As pointed out by J. Cary [9], Eq. (1) governs the motion of the particle oscillation center in the wave, whereas the fluid treatment is concerned only with the local particle velocity. The discrepancy is thus resolved by considering the fluid velocity flow shear between a particle's actual position and its oscillation center.

A third ponderomotive quantity, the ponderomotive force density, may be obtained by considering the momentum density fluid equation [10,11,12]. This quantity has been shown equivalent in effect to the fluid ponderomotive force [10], which indeed must be the case, since the two approaches contain the same physics. Expressions for the ponderomotive force in a magnetized plasma have also been derived by Statham and ter Haar [13], Cary and Kaufman [14], and others.

Some of the difficulties with the intuitive physical model now become clear. With at least three, and possibly more, forms of the ponderomotive force to choose from, the problem becomes one of which, if any, of these forces is the one actually counter-balancing the effective gravity. A seemingly reasonable criterion for distinguishing among these forces may be found by considering the physical mechanism usually associated with the interchange instability. The effective gravity driving the instability acts by inducing gravitational drifts which differ between electrons and ions. The resulting charge separation in the presence of an azimuthal density perturbation produces an $\mathbf{E} \times \mathbf{B}$ drift which reinforces the perturbation. We might then ask which of these ponderomotive forces influences by its induced drifts the charge separation obtained in the presence of a perturbation. There are again complications however, this time because the meaning of charge separation is unclear in the quasineutral formulations often used, and because RF-induced *density* as well as velocity perturbations can also lead to modifications in the gravitational current.

The wide variety of difficulties associated with the RF stabilization problem have led to a number of different theoretical approaches and therefore different viewpoints of the stabilizing mechanism.

D'Ippolito and Myra [11] have made a careful study of the stabilizing effects produced by applying the quasilinear approximation to the Vlasov-Maxwell equations to yield an effective ponderomotive force density. Kinetic effects such as wave energy absorption and resonant particle effects are therefore included in their version of the force. For the case of a left- (ion-) circularly polarized RF wave, without kinetic effects, it was again found that stabilizing effects occur only above ω_{ci}, while inclusion of the kinetic effects provided additional detail of the stabilizing influence of the RF wave when ω_0 was close to ω_{ci}.

Cohen and Rognlien [10] have developed a two-fluid model in which the stabilizing characteristics of both ponderomotive and sideband effects are included. When ponderomotive effects are considered, the model produces stability criteria identical to those obtained by D'Ippolito and Myra in the fluid limit. Sideband effects, or effects generated as the result of the beating of the RF wave with high-frequency, RF-induced components of the interchange eigenmode, constitute yet another complication to the RF stabilization picture. In Cohen and Rognlien's analysis, these effects are found to produce an added stabilizing effect on both sides of ω_{ci} which is strongest against short-wavelength interchange modes and is dominant over ponderomotive stabilization when ω_0 is close enough to ω_{ci}.

A set of calculations due to McBride and co-workers has also considered sideband effects [15,16]. In these studies, a general formulation [17] requiring only the linear electron and ion susceptibilities and certain characteristics of the RF wave is implemented to find RF-induced modifications to the linear interchange dispersion relation. When non-resonant sidebands are assumed, it is found that stability occurs only when $\omega_0 < \omega_{ci}$, just the opposite result obtained from the ponderomotive calculations. Stabilization is, however, obtained for $\omega_0 > \omega_{ci}$ when resonant sidebands are assumed. In another study conducted recently by Myra and D'Ippolito, the effects of sidebands were found to partially cancel previously calculated ponderomotive effects [18].

A different approach was taken by Similon and Kaufman [19] in their study of the problem. In their analysis, generalized ponderomotive forces were derived from functional

derivatives of a ponderomotive potential obtained from a two-timescale decomposition of the problem. Expressions for the electron and ion susceptibilities were evaluated assuming cold, uniform fluids for each species. These forces did not exhibit resonant behavior at the ion cyclotron frequency. Instead, the observed stability in Phaedrus when $\omega_0 > \omega_{ci}$ was attributed to the fact that slow wave resonances calculated for these forces for different propagation RF wavenumbers $\mathbf{k}_0$ always occurred at frequencies less than ω_{ci}. It was also found from an energy principle that the action of the interchange wave back on the RF wave is important in the stability analysis, yet another complicating feature of this problem.

With all the difficulties and complications associated with the theory of RF stabilization of interchange modes, there is much to be anticipated from the method of computer simulation. The problems associated with the importance of various effects and the relevance of various forms of the ponderomotive force are circumvented entirely, since all effects are calculated essentially from first principles and are thus followed to all orders in many of the usual expansion parameters. Interaction of sideband effects with ponderomotive effects are automatically treated, as is the self-consistent reaction of the interchange mode on the RF wave. Also, as is typical of the simulation method, diagnostics of most of the interesting dynamical quantities are readily available for analysis.

The simulation method applied here is unfortunately not without its own shortcomings. As currently run, only cold ions and electrons are employed, ruling out kinetic ion effects and electron-mediated electrostatic effects (e.g., ion sound waves). Periodic boundary conditions are used by the simulation, which leads to a somewhat unrealistic equilibrium model. The RF wave is loaded as an eigenmode of the system, rather than excited through the use of an antenna. The simulation magnetic field, which includes both the equilibrium and perturbed fields, is oriented perpendicular to the simulation plane. Both the RF wave and the interchange mode are thus constrained to perpendicular propagation. Direct comparison with most of the theories therefore cannot be made as the latter require appreciable parallel RF wave structure. Quantitative comparison with theories assuming the local approximation, $kL_n \gg 1$, k being the interchange wavenumber, is also infeasible, since $kL_n \sim 1$ or $kL_n \ll 1$ holds for all the simulation runs reported here. We find however that qualitative comparison to a theory of this type is reasonable, as will be demonstrated. It is also an unfortunate coincidence that cold plasma in the plane perpendicular to the background magnetic field does not support any ion-cyclotron-resonant RF waves. The only high-frequency wave present in this system is the fast compressional Alfvén wave, which is 100% electron-cyclotron polarized at the ion-cyclotron frequency. This rules out comparison with the results of the theories of D'Ippolito and Myra [11], Cohen and Rognlien [10], and McBride [15], each of which assumes either an ion-cyclotron- (left-) polarized RF wave, or cyclotron-resonant response of the ions to the RF wave. More recent analytical work by McBride and Stefan [20] considers the possible stabilizing influence of a perpendicularly propagating magnetosonic pump wave on interchange stability. Their calculation addresses only the effects of sideband coupling in the eikonal limit. Comparison of their results to our simulations is therefore not straightforward.

Despite all these deficiencies, a simulation of this type is still of considerable value. It is, after all, a clear working example of the interaction between a finite-amplitude RF wave

and the interchange mode. For example, the modification of the destabilizing gravitational current in the presence of RF can be and has been studied. Also, while the simulation model as presently implemented cannot be compared with current theories, neither have these theories as yet explored systems characterized by the parameters used here: ($kL_n \ll 1$, $kL_n \sim 1$, and $(k_\parallel)_{RF} = 0$). The case $kL_n \sim 1$ in particular is usually a difficult regime to study theoretically. Finally, it should be noted that none of the deficiencies mentioned here is inherent to the simulation method; some or all may be removed at some point in the future.

The balance of the paper is organized as follows. Model equations for the simulation and the related analysis are presented in the next section. We present some properties of these equations in Sec. III. The structure of the linear RF eigenmodes in our simulation model model is calculated in Sec. IV, wherein perturbations at second order in the RF amplitude are derived. We analytically address the linear stability of interchange modes in Sec. V, which is followed in Sec. VI by an eikonal theory of interchange stability in the presence of the RF wave. This theory suggests that the sum of electron and ion ponderomotive effects dominate sideband coupling in the eikonal limit for our model. We describe the initialization technique used in our simulations in Sec. VII and the simulation results in Sec. VIII. We observe a weak, partially stabilizing influence of the RF wave on the interchange modes. Some of the low-mode number simulation results are in remarkable agreement with the eikonal theory; this is discussed in Sec. IX. Simulation results and theory suggest that sideband coupling effects are more competitive with ponderomotive modifications for low mode number interchange modes. Future directions and a summary are given in Secs. X and XI, respectively.

II. THE MODEL EQUATIONS

We begin by studying some of the properties of the simulation equations. Some of these properties are derived to illustrate the nature of the simulation system we are using, while others are directly concerned with the stabilization process and will be checked against actual simulation results.

A number of features are required of a model suitable for the study of RF stabilization of interchange modes. The model must follow at least two spatial dimensions: one for the interchange propagation direction, and one for the inhomogeneity in the density gradient and RF field strength. Enough physics must be included to model both the low-frequency interchange mode and an RF wave in the ion-cyclotron frequency range. Neither the MHD formalism nor equations involving the guiding center approximation for the ions may therefore be used.

At the same time, as a matter of practicality, a workable model should also exclude certain features. Inclusion of electron or speed-of-light timescales would require unacceptably small simulation timesteps. The electron timescale may be eliminated by representing the electrons as a cold $\mathbf{E} \times \mathbf{B}$ fluid and assuming quasineutrality, while the speed of light timescale may be avoided by ignoring the displacement current relative to the plasma current (the Darwin approximation). It is also desirable as a first attempt to use only cold ions.

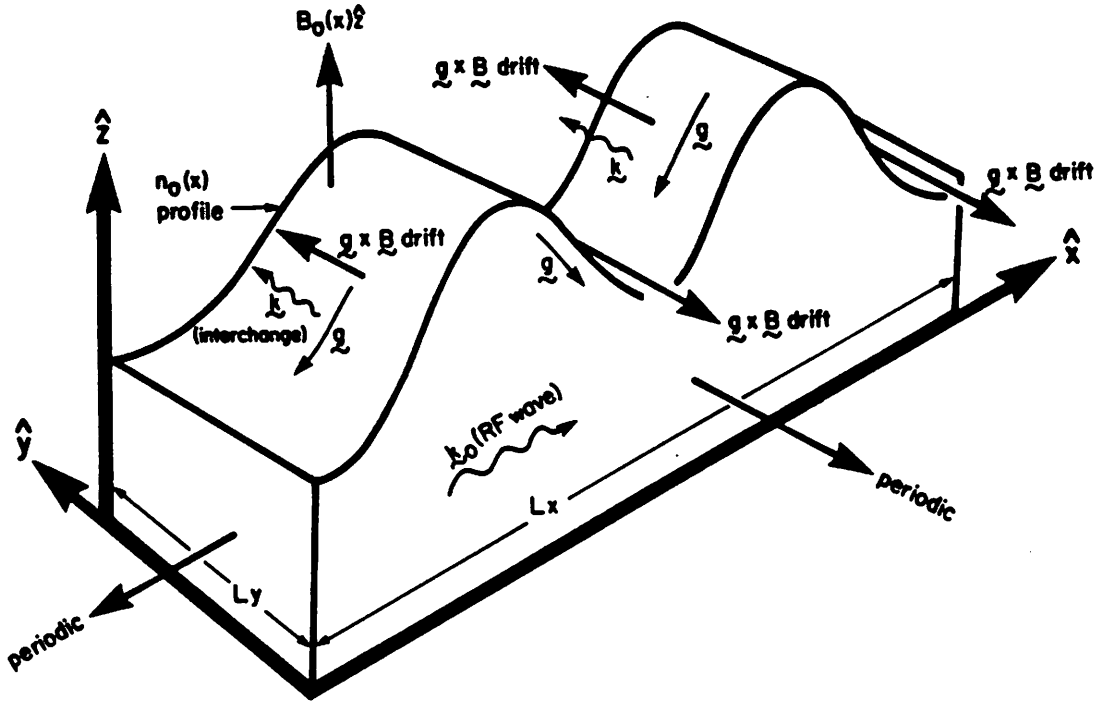

FIG. 1. Schematic of the simulation model. The time-independent equilibrium consists of the double-peaked density profile $n_0(x)$, the static gravitational acceleration field $\mathbf{g}(x) = g(x)\hat{\mathbf{x}}$, the time-independent magnetic field $\mathbf{B}_0(x) = B_0(x)\hat{\mathbf{z}}$, and the $\mathbf{g} \times \mathbf{B}$ ion gravitational drift, $-mcg/eB_0\hat{\mathbf{y}}$. The "modified" equilibrium is composed of the time-independent equilibrium plus the standing RF wave with propagation vector $\mathbf{k}_0(x) = k_0(x)\hat{\mathbf{x}}$. The interchange mode, excited by a small perturbation at the beginning of the simulation, typically propagates in the $\hat{\mathbf{y}}$-direction.

Warm ions are essential in our problem only through their role in producing the effective centrifugal force via parallel streaming along curved field lines in mirror geometry. This effect may be modeled with an external gravity, eliminating the need for warm ions. Use of cold ions greatly reduces the number of ion particles that would otherwise be required to fill the velocity dimensions of ion phase space.

The simulation code, ZEN [21], a 2-d modification of the 2 1/2-d quasineutral Darwin code PEPSI described in a previous report [22], fits these specifications. A schematic of the simulation model is shown in Fig. 1. Simulations take place in the x-y plane perpendicular to the magnetic field $B(x,y,t)\hat{\mathbf{z}}$, which is dynamically followed in time. The RF wave propagation vector $\mathbf{k}_0(x)$, the equilibrium density gradient $\nabla n_0(x)$, and an external gravitational field $\mathbf{g}(x)$ are all initialized to point in the $\pm\hat{\mathbf{x}}$-direction, while a small inter-

change perturbation is initialized with a sinusoidal dependence in the $\hat{\mathbf{y}}$-direction. Full ion dynamics are included in the code, and $n_e = n_i$ and $\mathbf{u}_e = c\mathbf{E} \times \mathbf{B}/B^2$ are assumed for the electron density and fluid velocity respectively.

The algorithm used by our simulations may be represented by the fluid equations :

$$\frac{\partial \mathbf{u}}{\partial t} + \mathbf{u} \cdot \nabla \mathbf{u} = \frac{e}{m}\left(\mathbf{E} + \frac{\mathbf{u} \times \mathbf{B}}{c}\right) + \mathbf{g}, \tag{5a}$$

$$\frac{\partial n}{\partial t} = -\nabla \cdot (n\mathbf{u}), \tag{5b}$$

$$\frac{\partial \mathbf{B}}{\partial t} = -c\nabla \times \mathbf{E}, \tag{5c}$$

$$\mathbf{E} = \left(\frac{\nabla \times \mathbf{B}}{4\pi e n} - \frac{\mathbf{u}}{c}\right) \times \mathbf{B}, \tag{5d}$$

where $\mathbf{u}$ is the *ion* fluid velocity, $n = n_i = n_e$ is the density, and again, m is the *ion* mass. Equation (5d) comes from the zero-pressure, inertialess electron momentum equation

$$0 = \mathbf{E} + \frac{\mathbf{u}_e \times \mathbf{B}}{c}, \tag{6}$$

where for $\mathbf{u}_e$, Ampère's Law has been substituted neglecting the displacement current. Periodic boundary conditions are enforced in both the x- and y-directions.

The particle ions of this simulation model actually obey

$$\frac{d\mathbf{v}}{dt} = \frac{e}{m}\left(\mathbf{E} + \frac{\mathbf{v} \times \mathbf{B}}{c}\right) + \mathbf{g}, \tag{7}$$

where $\mathbf{v}$ is the particle velocity; however, the fluid ion momentum equation (5a) is appropriate since the simulations reported here are initialized with cold ions which remain cold through the usable portion of the simulation.

Since the simulation takes place in the x-y plane, the magnetic field need only have a z-component: $\mathbf{B} = B(x, y, t)\hat{\mathbf{z}}$. Noting also that $\mathbf{E}$ only appears in the combination $\mathbf{E} + \mathbf{u} \times \mathbf{B}/c$, Eqs. (5) may be simplified to

$$\frac{\partial \mathbf{u}}{\partial t} + \mathbf{u} \cdot \nabla \mathbf{u} = -\frac{B\nabla B}{4\pi m n} + \mathbf{g}, \tag{8a}$$

$$\frac{\partial n}{\partial t} = -\nabla \cdot (n\mathbf{u}), \tag{8b}$$

$$\frac{\partial B}{\partial t} = -\nabla \cdot (B\mathbf{u}) + \frac{cB}{4\pi e}\hat{\mathbf{z}} \cdot \nabla\left(\frac{1}{n}\right) \times \nabla B, \tag{8c}$$

where $\mathbf{u} = (u_x, u_y, 0)$. Equations (8) form the basis for all subsequent analysis in this report.

III. PROPERTIES OF THE EQUATIONS

Several properties may be derived for the system described by Eqs. (8). A number of these properties are particularly appealing because they have a simple physical interpretation.

From Ampère's Law, the electron fluid velocity may be expressed as

$$\mathbf{u}_e = \mathbf{u} - \frac{c}{4\pi en}\nabla B \times \hat{\mathbf{z}}, \tag{9}$$

from which immediately follows $\mathbf{J} \cdot \nabla B = 0$ and $\nabla \cdot \mathbf{J} = 0$, as is also true in MHD theory. The total current thus flows along constant-B contours and is divergence-free.

Substituting Eq. (9) into Eq. (8b) yields

$$\frac{\partial n}{\partial t} = -\nabla \cdot (n\mathbf{u}_e), \tag{10}$$

the electron continuity equation, while substitution into Eq. (8c) produces

$$\frac{\partial B}{\partial t} = -\nabla \cdot (B\mathbf{u}_e), \tag{11}$$

demonstrating conservation of the magnetic flux $\int B\,dx\,dy$. Equations (8a), (9), (10), and (11) are an alternative and equivalent set of equations to Eqs. (8). The similarity of Eqs. (10) and (11) may be exploited to yield

$$\left(\frac{\partial}{\partial t} + \mathbf{u}_e \cdot \nabla\right)\left(\frac{B}{n}\right) = 0, \tag{12}$$

i.e., the ratio B/n is constant in the electron fluid frame. Thus, the magnetic field may be thought of as being frozen into the electrons.

An energy conservation theorem also exists for this system. Taking the dot product of both sides of Eq. (8a) with $mn\mathbf{u}$ produces

$$\frac{1}{2}mn\frac{\partial u^2}{\partial t} + \frac{1}{2}mn\mathbf{u} \cdot \nabla u^2 = -\frac{1}{4\pi}\mathbf{u}B \cdot \nabla B + mn\mathbf{u} \cdot \mathbf{g}. \tag{13}$$

Ampère's Law (Eq. (9)) may be used to show

$$\mathbf{u}B \cdot \nabla B = \mathbf{u}_e B \cdot \nabla B. \tag{14}$$

Multiplying both sides of Eq. (11) by B yields

$$\mathbf{u}_e B \cdot \nabla B = \frac{1}{2}\frac{\partial}{\partial t}(B^2) + \nabla \cdot (\mathbf{u}_e B^2). \tag{15}$$

Using ion continuity on the left side of Eq. (13) and substituting Eqs. (14) and (15), we obtain

$$\frac{\partial}{\partial t}\left(\frac{1}{2}nmu^2 + \frac{B^2}{8\pi} + nm\phi_g\right) + \nabla \cdot \left(\frac{1}{2}nmu^2\mathbf{u} + \frac{B^2}{4\pi}\mathbf{u}_e + nm\phi_g\mathbf{u}\right) = 0, \tag{16}$$

where $\mathbf{g} \equiv -\nabla\phi_g$. Thus the local total energy density defined as $nmu^2/2 + B^2/8\pi + nm\phi_g$ will be conserved in any region on the x-y plane up to a flux on the region boundary.

IV. THE RF WAVE

Estimates of the magnitudes of various quantities associated with the RF wave will be required for the stability analysis of the interchange mode when the RF wave is present. Since effects up to second order in the RF amplitude are expected to contribute to the main stabilizing influence, calculations to that order are performed. We use the equations

$$\frac{\partial u_x}{\partial t} + u_x \frac{\partial u_x}{\partial x} = -\frac{B}{4\pi m n}\frac{\partial B}{\partial x} + g, \tag{17a}$$

$$\frac{\partial u_y}{\partial t} + u_x \frac{\partial u_y}{\partial x} = 0, \tag{17b}$$

$$\frac{\partial n}{\partial t} = -\frac{\partial}{\partial x}(n u_x), \tag{17c}$$

$$\frac{\partial B}{\partial t} = -\frac{\partial}{\partial x}(B u_x), \tag{17d}$$

since the RF wave has been assumed to depend only on x.

Zero order. The equilibrium is assumed to be time-independent ($\partial/\partial t = 0$) with $u_x \equiv u_{x0} = 0$. Equation (17a) then implies a depression must exist in the magnetic field structure due to the gravity-induced current:

$$\frac{d}{dx}\left(\frac{B_0^2}{8\pi}\right) = m n_0 g, \tag{18}$$

while Eq. (17b) allows $u_{y0}(x)$ to be arbitrary. If we also require the electric field $\mathbf{E}_0$ to be zero in equilibrium, Eq. (5a) forces $u_{y0} = -mcg/eB_0$, the gravitational drift velocity. Equations (17c) and (17d) yield no further information.

First order. Equations (17a) through (17c) may be linearized about the equilibrium to yield a modified wave equation:

$$\frac{\partial^2}{\partial t^2}(u_{x1}B_0) = v_A^2(x)\left[\frac{1}{L_B}\left(\frac{1}{L_B} - \frac{1}{L_n}\right) + \frac{\partial^2}{\partial x^2}\right](u_{x1}B_0), \tag{19}$$

where u_{x1} is the first order component of u_x, $v_A^2 \equiv B_0^2/(4\pi m n_0)$, $L_B^{-1} \equiv (1/B_0)(\partial B_0/\partial x)$, and $L_n^{-1} \equiv (1/n_0)(\partial n_0/\partial x)$. Equation (17d) may be linearized to yield an equation for u_{y1} which evidently plays no role in the wave mechanics.

The lowest eigenmode (i.e., the mode with no spatial nodes) of Eq. (19) has a purely imaginary frequency when gravity is present and is probably more accurately described as a gravitational mode. This may be demonstrated using Sturm-Liouville theory [23] modified for periodic boundary conditions. When applied to Eq. (19), the condition

$$\omega_{(0)}^2 \le \frac{\int [|\partial\psi/\partial x|^2 - L_B^{-1}(L_B^{-1} - L_n^{-1})|\psi|^2]\, dx}{\int (|\psi|^2/v_A^2)\, dx}, \tag{20}$$

is obtained for the lowest eigenvalue $\omega_{(0)}^2$ for any trial function ψ expressible as a linear combination of the eigenmodes of Eq. (19), as demonstrated in Appendix A. By choosing

$\psi(x)$ = constant corresponding to an incompressible trial function, and assuming B_0 is a weak function of x (i.e., $L_B \gg L_n$), we find

$$\omega_{(0)}^2 \leq \frac{\int (g\, \partial n_0/\partial x)\, dx}{\int n_0\, dx}, \tag{21}$$

which is always negative in our gravitationally unstable system. Thus there always exists at least one unstable mode, and typically, it is unique.

The remaining eigenmodes of Eq. (19) are the compressional Alfvén modes which serve as RF waves in our simulations. For these modes, a uniform equilibrium ($L_B^{-1} = L_n^{-1} = 0$) will be assumed, because as stated earlier, only estimates of the wave quantities will be required. Assuming a standing wave of a given frequency ω_0 (this is the type of wave initially excited in the simulation), we find the following relative amplitudes and spatial and temporal phases among the wave components:

$$B_1 = \tilde{B} \sin k_0 x \cos \omega_0 t, \tag{22a}$$

$$n_1 = n_0 \frac{\tilde{B}}{B_0} \sin k_0 x \cos \omega_0 t, \tag{22b}$$

$$u_{x1} = - v_A \frac{\tilde{B}}{B_0} \cos k_0 x \sin \omega_0 t, \tag{22c}$$

$$u_{y1} = 0, \tag{22d}$$

$$E_{x1} = - \frac{k_0 B_0 \tilde{B}}{4\pi e n_0} \cos k_0 x \cos \omega_0 t, \tag{22e}$$

$$E_{y1} = - \frac{v_A}{c} \tilde{B} \cos k_0 x \sin \omega_0 t, \tag{22f}$$

where $k_0 \equiv \omega_0 / v_A$ is the wavenumber of the RF eigenmode.

Second order. When Eqs. (17a) and (17d) are expanded to second order and the uniform equilibrium assumption is again made, the result is

$$\frac{\partial^2}{\partial t^2}\left(\frac{B_2}{B_0}\right) = v_A^2 \frac{\partial^2}{\partial x^2}\left(\frac{B_2}{B_0}\right) - \frac{1}{2}\omega_0^2 \left(\frac{\tilde{B}}{B_0}\right)^2 \cos 2k_0 x (1 - 3 \cos 2\omega_0 t), \tag{23}$$

where expressions from Eqs. (22) have been used. This equation has a particular secular solution

$$\frac{B_2}{B_0} = -\frac{1}{8}\left(\frac{\tilde{B}}{B_0}\right)^2 \cos 2k_0 x (1 - 3\omega_0 t \sin 2\omega_0 t), \tag{24}$$

which has been observed in simulation as described in Sec. VIII. The d.c. portion of this solution is

$$\langle B_2 \rangle = -\frac{1}{8} B_0 \left(\frac{\tilde{B}}{B_0}\right)^2 \cos 2k_0 x. \tag{25}$$

The equation corresponding to Eq. (23) may be derived for u_{x2}; it has a secular solution whose d.c. part is

$$\langle u_{x2} \rangle = 0. \tag{26}$$

The expression for $\langle B_2 \rangle$ in Eq. (25) provides some insight into the nature of the second order current. Since $\langle u_{y0} \rangle = \langle u_{ey0} \rangle = \langle u_{y1} \rangle = 0$, we have

$$-\frac{\partial \langle B_2 \rangle}{\partial x} = \frac{4\pi}{c}\langle J_{y2} \rangle = \frac{4\pi e n_0}{c}\langle u_{y2} - u_{ey2} \rangle - \frac{4\pi e}{c}\langle n_1 u_{ey1} \rangle. \tag{27}$$

The last term in Eq. (27) may be evaluated using Eqs. (22):

$$-\frac{4\pi e}{c}\langle n_1 u_{ey1} \rangle = -\frac{1}{4}k_0 B_0 \left(\frac{\tilde{B}}{B_0}\right)^2 \sin 2k_0 x, \tag{28}$$

which we observe from Eq. (25) is equal to $-\partial \langle B_2 \rangle / \partial x$. Thus

$$\langle u_{y2} - u_{ey2} \rangle = 0, \tag{29}$$

which is somewhat of a surprise. We might have expected the second order current would be provided by a ponderomotive ion drift of the form

$$\langle u_{y2} \rangle = \frac{c\mathbf{F}_p \times \hat{\mathbf{z}}}{eB_0}, \tag{30}$$

where $\mathbf{F}_p$ is the ponderomotive force due to the RF wave; however if this is the case, it is canceled by the second order electron drift, and instead $\langle n_1 u_{ey1} \rangle$ must be considered as the important second-order current term. This type of electron current comes from the motion of electrons around a oscillation center. It is not clear whether this kind of second-order current will be of the type necessary to reverse the destabilizing gravitational current.

V. STABILITY OF THE INTERCHANGE WAVE

By considering the system containing the RF wave to be a *modified* equilibrium, it is possible to investigate the stability properties of the interchange mode in the presence of the wave. Assuming the interchange perturbation to be of the form $\delta n(x,y,t) = \delta n(x,t)e^{iky}$ (similarly for $\delta \mathrm{u}$ and δB), we obtain to first order

$$\left(\frac{\partial}{\partial t} + iku_y + \frac{\partial u_x}{\partial x}\right)\delta u_x = -G\frac{\delta B}{B} + G\frac{\delta n}{n} - u_x\frac{\partial \delta u_x}{\partial x} - \frac{v_A^2}{B}\frac{\partial \delta B}{\partial x} \tag{31a}$$

$$\left(\frac{\partial}{\partial t} + iku_y\right)\delta u_y = -ikv_A^2\frac{\delta B}{B} - \frac{\partial u_y}{\partial x}\delta u_x - u_x\frac{\partial \delta u_y}{\partial x} \tag{31b}$$

$$\frac{1}{n}\left(\frac{\partial}{\partial t} + iku_y + \frac{\partial u_x}{\partial x}\right)\delta n = -\frac{1}{n}\frac{\partial n}{\partial x}\delta u_x - ik\delta u_y - \frac{\partial \delta u_x}{\partial x} - \frac{u_x}{n}\frac{\partial \delta n}{\partial x} \tag{31c}$$

$$\frac{1}{B}\left(\frac{\partial}{\partial t} + iku_y + \frac{\partial u_x}{\partial x} + \frac{ikv_A^2}{\omega_{ci}}\frac{1}{n}\frac{\partial n}{\partial x}\right)\delta B = \frac{ikG}{\omega_{ci}}\frac{\delta n}{n} - \frac{G}{v_A^2}\delta u_x - ik\delta u_y - \frac{\partial \delta u_x}{\partial x} - \frac{u_x}{B}\frac{\partial \delta B}{\partial x} \tag{31d}$$

All equilibrium quantities in Eqs. (31) contain the RF wave and therefore have both space and time dependence. Here $\omega_{ci} \equiv eB/mc$ and $G \equiv g - \partial u_x/\partial t - u_x \partial u_x/\partial x$.

In the case of a vanishingly small RF wave, the assumptions $k^2 v_A^2 \ll \omega_{ci}^2$ and $\omega \ll \omega_{ci}$ in the local approximation yield the usual interchange dispersion relation

$$\bar{\omega}^2 + \frac{kg}{\omega_{ci}}\bar{\omega} + \frac{g}{n_0}\frac{\partial n_0}{\partial x}\frac{\tilde{\omega}_{ci}}{\omega_{ci}} = 0, \tag{32}$$

as expected, where $\bar{\omega} \equiv \omega - k u_{0y}$, ω is the interchange mode frequency, and $\tilde{\omega}_{ci} \equiv \omega_{ci} + \partial u_{0y}/\partial x$ is an effective ion cyclotron frequency.

When an RF wave is present, the eigenmode formalism may generalized by assuming the interchange perturbation quantities vary with time as

$$(\delta \mathbf{u}, \delta n, \delta B) = \sum_{m=-\infty}^{\infty} (\delta \mathbf{u}_m, \delta n_m, \delta B_m) \exp\left(-i(\omega + m\omega_0)t\right). \tag{33}$$

By again applying the local approximation, we find Eqs. (31) take the form

$$\sum_{m'} \mathcal{Q}_m^{m'} \cdot \delta \mathbf{q}_{m'} = 0, \tag{34}$$

where $\delta \mathbf{q} \equiv (\delta \mathbf{u}, \delta n, \delta B)$ and $\mathcal{Q}$ is an algebraic matrix quantity in both the four components of $\delta \mathbf{q}$ and in the index m, and depends only on the state of the modified equilibrium. The elements of $\mathcal{Q}$, $\mathcal{Q}_m^{m'}$, determine the strength of the RF-induced coupling between interchange sidebands m and m'. An eikonal theory of the RF modifications to the interchange dispersion relation is presented in the next section.

VI. EIKONAL STABILITY THEORY IN THE PRESENCE OF THE RF WAVE

The calculation formally presented by Eq. (34) may, for example, be performed for the case $kL_n \gg k_0 L_n \gg 1$. As indicated earlier, in the simulations performed for this study, $kL_n \sim k_0 L_n \sim 1$, so the simulation results cannot be expected to agree quantitatively with predictions from this calculation. We should expect qualitative agreement, however, since the simulation model and the calculation share much of the same physics. In particular, in both cases, the RF wave is a perpendicularly-propagating compressional Alfvén wave, and in both cases, there is no resonant enhancement at the ion-cyclotron frequency. The analysis should also be relevant to other particle simulations [24,25].

Figure 2 displays the slab configuration used for the calculation. Consider a compressional Alfvén pump wave with its spatial variation in the x direction perpendicular to the equilibrium magnetic field $\mathbf{B}_0 = B_0 \hat{z}$. There are time-varying electric fields $\mathbf{E}$ and fluxes for each species $\mathbf{\Gamma} = n\mathbf{u}$ (n is the number density and $\mathbf{u}$ is the fluid velocity) in the x-y plane. An equilibrium density gradient and a gravitational acceleration $\mathbf{g}$ to model magnetic field curvature are oriented in the x direction. The interchange mode varies only in the y direction in the eikonal limit.

We adopt the following assumptions and orderings:

$$\mathbf{B} \cdot \nabla = 0, \tag{35a}$$

$$|k_y| \gg |k_x| \gg |\nabla n^{(0)}/n^{(0)}|,\ |\nabla B_0/B_0|, \tag{35b}$$

$$m_i g \gg m_e g \sim 0, \tag{35c}$$

$$|\omega/\omega_0|,\ |\omega/(\omega_{ci} - \omega_0)| \ll |k_y n^{(0)}/\nabla n^{(0)}|^{-1} \ll 1, \tag{35d}$$

$$k_y g/\omega_{ci} \ll |\omega| \ll \omega_{ci}, \omega_0 \ll |\omega_{ce}|, \tag{35e}$$

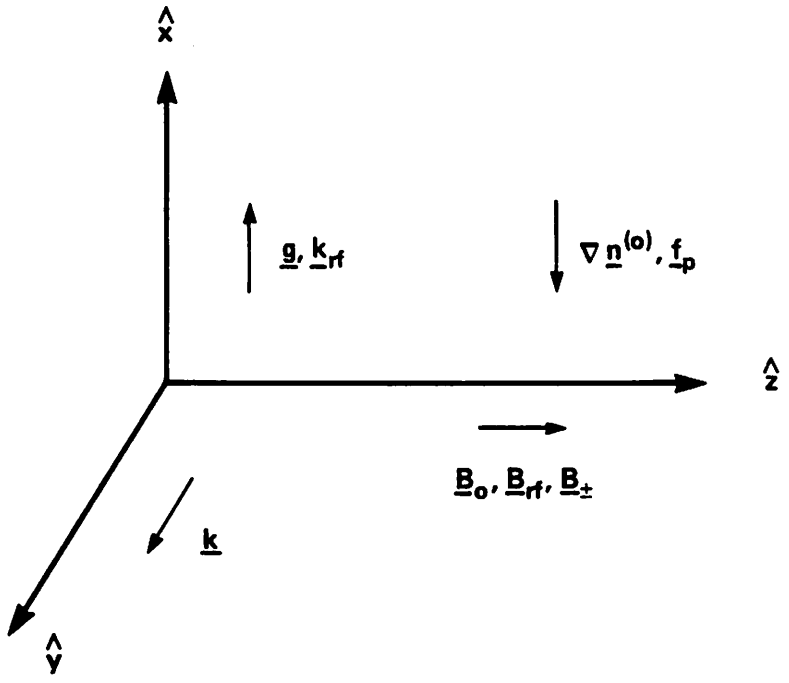

FIG. 2. Schematic of a cold-plasma slab with gravity. The wavenumber $\mathbf{k}$ shown indicates an interchange mode. There are time-varying electric fields, $\mathbf{E}_{RF}$ for the pump wave and $\mathbf{E}_{\pm}$ for the sidebands, in the x-y plane. There is a ponderomotive force $\mathbf{f}_p$ directed opposite to the gravity to help stabilize the interchange mode.

where $\mathbf{k} = (k_x, k_y)$ are the wave vectors in the calculation, ω is the complex angular frequency of the interchange mode, ω_0 is the pump-wave frequency, and ω_{ci} and ω_{ce} are the ion and electron cyclotron frequencies. Equation (35b) indicates that all waves are calculated in the eikonal limit.

The fluid analysis presented here is much like that used in Ref. 10. However, there are a number of important differences in the calculation undertaken and the assumptions made. The pump wave considered here is a compressional Alfvén wave, which is described fully self-consistently by Maxwell's equations and two-fluid equations in the Darwin quasi-neutral limit. No assumption is made regarding the polarization of the ion cyclotron sidebands coupled by the pump to the interchange wave beyond that implied by Fig. 2 and Eq. (35a). This is consistent with our simulation model and those of others [24,25]. Reference 10 did not consider compressional Alfvén pump waves and made very restrictive and artificial assumptions on the polarization and structure of the sidebands. The calculation presented is fully self-consistent and completely analytic, and treats ponderomotive and sideband coupling effects on an equal footing. The calculation and its results are new and not contained in previously reported research. Sideband coupling effects on interchange stability

in the presence of a compressional Alfvén wave have been addressed independently by McBride and Stefan with different ordering assumptions than those in Eq. (35).

The basic field equations in the quasi-neutral Darwin limit are

$$\nabla \times \mathbf{E} = -\frac{1}{c}\frac{\partial}{\partial t}\mathbf{B}, \tag{36a}$$

$$\nabla \times \mathbf{B} = \frac{4\pi}{c}\mathbf{J}, \tag{36b}$$

$$\nabla \cdot \mathbf{J} = 0, \tag{36c}$$

$$\nabla \cdot \mathbf{B} = 0, \tag{36d}$$

where $\mathbf{E}$ and $\mathbf{B}$ are the total electric and magnetic fields and $\mathbf{J}$ is the current density. The cold fluid equations are

$$\frac{\partial n_s}{\partial t} + \nabla \cdot \mathbf{\Gamma}_s = 0, \qquad s = i, e, \tag{37a}$$

$$m_i \frac{\partial}{\partial t}\mathbf{\Gamma}_i = -m_i \nabla \cdot \left(\frac{\mathbf{\Gamma}_i \mathbf{\Gamma}_i}{n_i}\right) + e n_i \mathbf{E} + \frac{e\mathbf{\Gamma}_i \times \mathbf{B}}{c} + n_i m_i \mathbf{g}, \tag{37b}$$

$$-e\left(n_e \mathbf{E} + \frac{\mathbf{\Gamma}_e \times \mathbf{B}}{c}\right) = 0, \tag{37c}$$

$$\mathbf{J} = e(\mathbf{\Gamma}_i - \mathbf{\Gamma}_e), \tag{37d}$$

where n_s are the species number densities, $\mathbf{\Gamma}_s$ are the flux densities, and e is the ion charge (singly charged). These equations are equivalent to Eqs. (5). All the dependent variables are decomposed into a superposition of modes at the different frequencies:

$$\mathbf{\Gamma}_s = \mathbf{\Gamma}_s^{(0)} + \mathbf{\Gamma}_s(\omega_0) + \mathbf{\Gamma}_s(\omega) + \mathbf{\Gamma}_s(\omega + \omega_0) + \mathbf{\Gamma}_s(\omega - \omega_0) + \mathbf{\Gamma}_s^{(2)}, \tag{38}$$

where the (0) and (2) superscripts indicate time-independent equilibrium and second order (in the pump-wave amplitude) quantities and the remaining components are linear in the pump wave, sideband, and interchange amplitudes.

We again find the equilibrium force-balance condition in the absence of the RF source

$$-\frac{\partial}{\partial x}\frac{B_0^2}{8\pi} + n^{(0)} m_i g = 0, \tag{39}$$

and, hence, the equilibrium ion flux

$$\mathbf{\Gamma}_i^{(0)} = -\frac{n^{(0)} g}{\omega_{ci}}\hat{\mathbf{y}}. \tag{40}$$

An equation for low frequency interchange modes can then be obtained by linearizing and summing Eqs. (37b) and (37c), by taking the cross product with $c\mathbf{B}_0/B_0^2$, and by calculating the divergence of the equation using $\nabla \cdot \mathbf{J} = 0$:

$$\nabla \cdot \left\{\frac{c\mathbf{B}_0}{B_0^2} \times \left[-m_i \frac{d}{dt}\mathbf{\Gamma}_i(\omega) + n_i(\omega) m_i \mathbf{g} + \delta \mathbf{f}_p + \delta \mathbf{f}_{sb}\right]\right\} = 0, \tag{41}$$

where $\delta \mathbf{f}_p$ and $\delta \mathbf{f}_{sb}$ are the low frequency linearized ponderomotive and sideband force densities whose calculation follows. At this point, the equilibrium quantities formally contain small perturbative shifts arising from the time-averaged second-order ponderomotive RF effects calculated in Ref. 10. As argued in Ref. 10, these shifts have a negligible effect on Eq. (41) compared to $\delta \mathbf{f}_p$ and $\delta \mathbf{f}_{sb}$. We now introduce the linear incompressible fluid displacement vector $\boldsymbol{\xi}$ and use continuity (37a) to obtain

$$\boldsymbol{\Gamma}_i(\omega) = -i\omega n^{(0)} \boldsymbol{\xi}, \tag{42a}$$

and

$$n_i(\omega) = -\boldsymbol{\xi} \cdot \nabla n^{(0)}. \tag{42b}$$

With the orderings given in (35), Eq. (41) leads to

$$\frac{c}{B_0}\frac{\partial}{\partial y}\left(n^{(0)} m_i \omega^2 - \frac{\partial n^{(0)}}{\partial x} m_i g\right) \xi_x + \nabla \cdot \left[\frac{c\mathbf{B}_0}{B_0^2} \times (\delta \mathbf{f}_p + \delta \mathbf{f}_{sb})\right] = 0. \tag{43}$$

We next derive $\delta \mathbf{f}_s$ and $\delta \mathbf{f}_{sb}$, and follow this with a calculation of the compressional Alfvén pump-wave fields for use in evaluating $\delta \mathbf{f}_p$ and $\delta \mathbf{f}_{sb}$ in Eq. (43). Calculating $\delta \mathbf{f}_p$ and $\delta \mathbf{f}_{sb}$ is somewhat simplified by the fact that all nonlinearities are contained in Eqs. (37b) and (37c). Equation (37a) trivially relates n_s and $\boldsymbol{\Gamma}_s$, and (37d) determines $\mathbf{J}$ from $\boldsymbol{\Gamma}_s$. The linearly perturbed ponderomotive force density comes from the combination of kinetic stress and Lorentz force terms [5,6,10,18,26],

$$\delta \mathbf{f}_p = \delta \sum_s \left[-m_s \nabla \cdot \left\langle \frac{\boldsymbol{\Gamma}(\omega_0)\boldsymbol{\Gamma}(\omega_0)}{n^{(0)}} \right\rangle_s + q_s \left\langle \frac{\boldsymbol{\Gamma}_s(\omega_0) \times \mathbf{B}(\omega_0)}{c} \right\rangle\right], \tag{44}$$

where $\delta = n(\omega)(\partial/\partial n^{(0)})$ at low plasma pressure and $\langle\ \rangle$ indicates a time average. With the use of Eqs. (36b), (37d), and (42b), Eq. (44) becomes

$$\begin{aligned} \delta \mathbf{f}_p =& m_i \nabla \cdot \left[\frac{\xi_x}{n^{(0)}}\left(\frac{\partial n^{(0)}}{\partial x}\right)\left\langle \frac{\boldsymbol{\Gamma}_i(\omega_0)\boldsymbol{\Gamma}_i(\omega_0)}{n^{(0)}} \right\rangle\right] \\ & - \frac{\xi_x}{n^{(0)}}\left(\frac{\partial n^{(0)}}{\partial x}\right)\left\langle \frac{(\nabla \times \mathbf{B}(\omega_0)) \times \mathbf{B}(\omega_0)}{4\pi} \right\rangle, \end{aligned} \tag{45}$$

for pump-wave electric fields polarized perpendicular to $\mathbf{B}_0$ and $m_e/m_i \to 0$.

The linearized low frequency force density due to sideband coupling is deduced from the use of Eqs. (37b) and (37c) and the quasineutrality condition,

$$\begin{aligned} \delta \mathbf{f}_{sb} =& \sum_{\pm} -m_i \nabla \cdot \left[\frac{\boldsymbol{\Gamma}_i(\omega_0)\boldsymbol{\Gamma}_i(\omega \pm \omega_0)}{n^{(0)}} + \frac{\boldsymbol{\Gamma}_i(\omega \pm \omega_0)\boldsymbol{\Gamma}_i(\omega_0)}{n^{(0)}}\right] \\ & + \frac{(\nabla \times \mathbf{B}(\omega_0)) \times \mathbf{B}(\omega \pm \omega_0)}{4\pi} + \frac{(\nabla \times \mathbf{B}(\omega \pm \omega_0)) \times \mathbf{B}(\omega_0)}{4\pi}. \end{aligned} \tag{46}$$

Algebraic reduction of Eq. (45) requires calculation of $\Gamma_s(\omega \pm \omega_0)$ from Eqs. (37b) and (37c). We obtain

$$q_s \Gamma_s(\omega_\pm) = \sigma_s \cdot \left\{ \mathbf{E}(\omega_\pm) - \frac{m_s}{n^{(0)} q_s} \nabla \cdot \left[\frac{\Gamma_s(\omega)\Gamma_s(\omega_0)}{n^{(0)}} + \frac{\Gamma_s(\omega_0)\Gamma_s(\omega)}{n^{(0)}} \right] + \frac{1}{n^{(0)}} \left[n_s(\omega)\mathbf{E}(\omega_0) + n_s(\omega_0)\mathbf{E}(\omega) \right] + \frac{\Gamma_s(\omega) \times \mathbf{B}(\omega_0)}{n^{(0)} c} \right\}, \tag{47}$$

with $\mathbf{B}(\omega) = 0$ for electrostatic interchange modes and

$$\sigma_s(\omega_\pm) = \frac{\omega_{ps}^2}{4\pi(\omega_{cs}^2 - \omega_\pm^2)} \begin{pmatrix} -i\omega_\pm & -\omega_{cs} \\ \omega_{cs} & -i\omega_\pm \end{pmatrix}, \tag{48}$$

where $\omega_\pm \equiv \omega \pm \omega_0$ and $\omega_{cs} = q_s B_0 / m_s c$. With the use of (35a) and (42b), Eq. (47) simplifies to

$$q_s \Gamma_s(\omega_\pm) = \sigma_s(\omega_\pm) \cdot \left[\mathbf{E}(\omega_\pm) - \frac{\xi_x}{n^{(0)}} \frac{\partial n^{(0)}}{\partial x} \mathbf{E}(\omega_0) \right], \tag{49}$$

in agreement with Refs. 18 and 26. The sideband electric fields are determined by the eikonal wave equation derived from Eqs. (36a), (36b), and (49),

$$\begin{aligned} \mathbf{D}(\omega_\pm) \cdot \mathbf{E}(\omega_\pm) &\equiv \left[k_y^2 c^2 \hat{\mathbf{x}}\hat{\mathbf{x}} - i4\pi\omega_\pm \sum_s \sigma_s(\omega_\pm) \right] \cdot \mathbf{E}(\omega_\pm) \\ &= -i4\pi\omega_\pm \frac{\xi_x}{n^{(0)}} \left(\frac{\partial n^{(0)}}{\partial x} \right) \sum_s \sigma_s(\omega_\pm) \cdot \mathbf{E}(\omega_0) \\ &= -i\omega_\pm \frac{\xi_x}{n^{(0)}} \left(\frac{\partial n^{(0)}}{\partial x} \right) c\nabla \times \mathbf{B}(\omega_0). \end{aligned} \tag{50}$$

The sideband magnetic field is given by

$$\mathbf{B}(\omega_\pm) = \frac{c}{i\omega_\pm} \nabla \times \mathbf{E}(\omega_\pm). \tag{51}$$

The pump-wave electromagnetic fields satisfy the linearized wave equation with no antenna structure present,

$$\mathbf{D}_0 \cdot \tilde{\mathbf{E}}(\omega_0) \equiv \left[c^2 \frac{\partial^2}{\partial x^2} \hat{\mathbf{y}}\hat{\mathbf{y}} + i4\pi\omega_0 \sum_s \sigma_s(\omega_0) \right] \cdot \tilde{\mathbf{E}}(\omega_0) = 0, \tag{52}$$

where

$$i4\pi\omega_0 \sum_s \sigma_s(\omega_0) = \frac{\omega_0^2 \omega_{pi}^2}{\omega_{ci}^2 - \omega_0^2} \begin{pmatrix} 1 & -i\omega_0/\omega_{ci} \\ i\omega_0/\omega_{ci} & 1 \end{pmatrix}, \tag{53}$$

$\mathbf{E}(\omega_0) = \frac{1}{2}\tilde{\mathbf{E}}(x)\exp(-i\omega_0 t) + \text{c.c.}$, and $\mathbf{B}(\omega_0)$ is similarly defined. We assume that the RF pump wave has no y variation to be consistent with the simulation model and that

its variation in x is more rapid than the plasma equilibrium variation. The pump-wave dispersion relation resulting from Eq. (52) is

$$\det \mathbf{D}_0 = \frac{\omega_0^2 \omega_{pi}^2}{\omega_{ci}^2 - \omega_0^2}\left(k_x^2 c^2 - \frac{\omega_0^2 \omega_{pi}^2}{\omega_{ci}^2}\right) = 0, \tag{54}$$

i.e., $\omega_0^2 = k_x^2 v_A^2$, where $\partial^2/\partial x^2 = -k^2$ and $v_A = c\omega_{ci}/\omega_{pi}$ is the Alfvén velocity.

As a result of Eqs. (53) and (54), $\tilde{E}_x(\omega_0)/\tilde{E}_y(\omega_0) = i\omega_0/\omega_{ci}$, which gives a right circularly polarized wave at ion cyclotron resonance. The ion flux density components of the pump wave are

$$\hat{\mathbf{x}} \cdot \tilde{\mathbf{\Gamma}}_i(\omega_0) = -\frac{\omega_{pi}}{8\pi e \omega_{ci}} \tilde{E}_y(\omega_0), \qquad \hat{\mathbf{y}} \cdot \tilde{\mathbf{\Gamma}}_i(\omega_0) = 0; \tag{55}$$

and the pump-wave magnetic field amplitude follows from

$$\tilde{B}_z(\omega_0) = \frac{c}{i\omega_0}\frac{\partial}{\partial x}\tilde{E}_y(\omega_0). \tag{56}$$

Use of Eqs. (48) to (56) yields

$$\hat{\mathbf{y}} \cdot \tilde{\mathbf{\Gamma}}_i(\omega_\pm) = \pm\frac{i\omega_0}{8\pi e}\frac{\omega_{pi}^2}{\omega_{ci}^2}\frac{k_y^2 v_A^2}{\omega_0^2 - k_y^2 v_A^2}\frac{\xi_x}{n^{(0)}}\left(\frac{\partial n^{(0)}}{\partial x}\right)\tilde{E}_y(\pm\omega_0), \tag{57a}$$

and

$$\hat{\mathbf{x}} \cdot \tilde{\mathbf{\Gamma}}_i(\omega_\pm) = 0, \tag{57b}$$

where $\tilde{E}_y(-\omega_0) \equiv \tilde{E}_y(\omega_0)^*$ and $\omega_\pm \equiv \pm\omega_0$ for $|\omega| \ll |\omega_0 - \omega_{ci}|$. The sideband electric-field polarizations are determined by Eq. (50) and are right circular for $\omega_0 = \omega_{ci}$. Because $\omega_0^2 = k_x^2 v_A^2 \ll k_y^2 v_A^2$, the sideband perturbations are *not* normal modes.

We can now explicitly evaluate $\delta\mathbf{f}_p$ and $\delta\mathbf{f}_{sb}$, Eqs. (44) and (45), and subsequently $\nabla \cdot [c\mathbf{B}_0 \times (\delta\mathbf{f}_p + \delta\mathbf{f}_{sb})/B_0^2]$. We note that there is some dependence on the waveform of the pump wave (plane wave or standing wave) and that cancellation of leading order terms in the eikonal expansion tends to occur. Here we consider standing-wave pumps and calculate $\delta\mathbf{f}_p$ and $\delta\mathbf{f}_{sb}$ through zero and first order in $|k_x/k_y| \ll 1$. The perturbed ponderomotive force density δf_p has only a finite x component, and its calculation is straightforward. However, in our configuration the derivation of the sideband coupling is more subtle: $\delta\mathbf{f}_{sb}$ becomes

$$\delta\mathbf{f}_{sb} = \sum_{\pm} -m_i \nabla \cdot \left[\frac{\mathbf{\Gamma}_i(\omega_0)\mathbf{\Gamma}_i(\omega_\pm)}{n^{(0)}} + \frac{\mathbf{\Gamma}_i(\omega_\pm)\mathbf{\Gamma}_i(\omega_0)}{n^{(0)}}\right] - \nabla_\perp\left[\frac{B_z(\omega_0)B_z(\omega_\pm)}{4\pi}\right]. \tag{58}$$

The second set of terms on the right side of (58) involving magnetic perturbations contributes negligibly to Eq. (43) compared to ponderomotive terms as a result of $\nabla_\perp \cdot (\hat{\mathbf{z}} \times \nabla_\perp) \equiv 0$ and Eq. (35). Furthermore, as a consequence of Eqs. (55) and (57), the contributions to Eq. (43) from the kinetic stress terms in $\delta\mathbf{f}_{sb}$ are also negligible in the eikonal limit.

Thus, we obtain a negligible contribution to interchange stability from $\delta \mathbf{f}_{sb}$ and

$$\delta \mathbf{f}_p = \hat{\mathbf{x}} m_i \frac{\partial}{\partial x}\left[\frac{\xi_x}{n^{(0)}}\left(\frac{\partial n^{(0)}}{\partial x}\right)\left\langle \frac{\Gamma_{ix}(\omega_0)\Gamma_{ix}(\omega_0)}{n^{(0)}}\right\rangle\right] + \hat{\mathbf{x}}\frac{\xi_x}{n^{(0)}}\left(\frac{\partial n^{(0)}}{\partial x}\right)\frac{\partial}{\partial x}\left\langle \frac{B_z(\omega_0)^2}{8\pi}\right\rangle$$

$$\approx \hat{\mathbf{x}}\frac{\omega_{pi}^2}{\omega_{ci}^2}\frac{\xi_x}{n^{(0)}}\left(\frac{\partial n^{(0)}}{\partial x}\right)\frac{\partial}{\partial x}\frac{|\tilde{E}_y(\omega_0)|^2}{16\pi}, \tag{59}$$

for a standing-wave pump. The linearly perturbed ponderomotive force density is directed opposite to the perturbed gravitational force and is stabilizing in its effect on the interchange mode if the RF electric field amplitude gradient is positive in Eq. (59). The resulting interchange stability condition obtained from Eqs. (43) and (59) can be written in the form

$$\frac{\partial}{\partial x}\left\langle \frac{B_z(\omega_0)^2}{8\pi}\right\rangle > n^{(0)} m_i g = \frac{\partial}{\partial x}\left(\frac{B_0^2}{8\pi}\right). \tag{60}$$

We have made use of the equilibrium force-balance relation Eq. (38) on the right side of Eq. (60) to emphasize the relative magnitude of the RF force required for stabilization. We note the complete absence of cyclotron resonances in our final expressions, and there is no dependence on the sign of $\omega_0 - \omega_{ci}$. Furthermore, the results obtained depend crucially on the self-consistent calculation of the RF pump-wave field pattern through the amplitude gradients appearing in the results and the use of the pump-wave dispersion relation and polarization characteristics at several steps in the derivation.

We thus conclude from our eikonal theory that compressional Alfvén waves with variation exactly perpendicular to the equilibrium magnetic field alter interchange stability through the ponderomotive force exerted on the plasma. There is no resonant enhancement found when the frequency of the applied RF is near the ion cyclotron frequency. Because there is no resonant dielectric enhancement of the nonlinear effects, stabilization of interchange modes by a compressional Alfvén wave is *not* efficient, a result that confirms the philosophy of and the experience in a number of experiments [1,3,4].

VII. INITIALIZATION OF THE SIMULATION

With the basic characteristics and expected behavior of the model equations established, we next turn to an examination of the simulation model itself. As already indicated, the computer code used for simulations in this study is a modification of the PEPSI code, described elsewhere [22]. The main timestep-loop algorithm used here differs only by the inclusion of the static gravitational acceleration field $\mathbf{g}(x)$. Apart from this addition and the extensive alterations made to the diagnostics routines, the principal difference between the present code ZEN and PEPSI lies in the algorithm used to initialize the simulations.

The process of initializing the simulations follows in three stages the three natural divisions in the model suggested by the analysis. First, the time-independent equilibrium is established. The force due to the gradient in the gravitational field is exactly canceled by the Lorentz force acting on the ion gravitational drift. Second, the RF wave in the form of a linear compressional Alfvén eigenmode is calculated and incorporated to form the "modified" equilibrium. Finally, a small interchange perturbation is excited.

A typical time-independent equilibrium is illustrated schematically in Fig. 1. The initial unperturbed ion particle positions are chosen to lie in a rectangular grid pattern non-uniformly spaced in the x-direction to form two peaks in the density profile. The fixed gravity is defined at each point on a regularly-spaced permanent rectangular grid (not to be confused with the grid on which the particles are loaded, which is temporary) to point antiparallel to the initial density gradient. This guarantees the system will be initially interchange-unstable. Specifically, we have taken

$$n_0(x) = n_0 - (n_0 - n_l)\cos\frac{4\pi x}{L_x}, \tag{61}$$

and

$$g(x) = -g_0 \sin\frac{4\pi x}{L_x}, \tag{62}$$

where n_0, n_l, and g_0 are user-adjustable parameters. The equilibrium thus depends on x only. The equilibrium magnetic field may then be calculated on the (permanent) grid from

$$B_0(x) = \left\{ B_0^2(0) + \frac{1}{2} m n_0 g_0 L_x \left[4\left(\cos\frac{4\pi x}{L_x} - 1\right) - \left(1 - \frac{n_l}{n_0}\right)\left(\cos\frac{8\pi x}{L_x} - 1\right)\right]\right\}^{1/2}, \tag{63}$$

which is a consequence of the force balance equation (18). The ion particles are loaded next according to the inverse-cumulative distribution function corresponding to Eq. (61). The magnetic field and gravity are calculated at the position of each particle by applying the same linear weighting scheme used in the main timestep loop. We define the electric fields E_x and E_y and the particle x-velocities to be zero initially, allowing the particle drifts in the y-direction to be chosen so that the resulting Lorentz force cancels the gravitational force.

Each of the density peaks represents the essential features of an interchange-unstable mirror plasma equilibrium. The $\hat{z}$-axis represents the axial direction in mirror geometry; the $\hat{x}$- and $\hat{y}$-axes then correspond to the radial and azimuthal directions respectively. The external gravity $g(x)$ plays the role of the destabilizing centrifugal force generated by bad field-line curvature in mirror geometry.

The periodic boundary conditions prevent us from drawing direct geometric analogies between features of our simulation equilibrium and those of a mirror system. These boundary conditions are the natural choice for the (azimuthal) y-direction, but they are somewhat awkward when applied to the (radial) x-direction. If a single density peak were present in the system, the simulation could be considered to be a slab-geometry representation of the mirror system. However, for reasons involving the RF wave described below, we are required to load two density peaks in the system and then the analogy between the mirror system and the simulation system becomes less clear. We might regard each of the two density peaks as separate slab systems if the two systems do not interact, although even then the presence of periodic boundary conditions in the (radial) x-direction are grounds for suspicion. The simulations thus do not attempt to model mirror geometry directly and should instead be considered generic to the study of the RF stabilization mechanism.

After the equilibrium is loaded, the RF wave is installed in the form of a compressional Alfvén eigenmode of the system. Earlier versions of the code incorporated antennas as sources of the RF wave; however, difficulties were encountered in establishing a steady state since compressional Alfvén waves propagate undamped in this system. Problems were also created by the strong field gradients in the vicinity of the antennas.

The spatial structure of the eigenmode is found by solving numerically the finite-difference version of the eigenvalue wave equation

$$v_{A0}^2(x)\frac{\partial^2 B_1}{\partial x^2} = -\omega^2 B_1, \tag{64}$$

where $v_{A0}^2(x) \equiv B_0^2(x)/4\pi m n_0(x)$. Thus at present, the RF eigenmode also depends on x only. Technically, Eq. (19) should be solved to obtain the linear RF eigenmodes of the

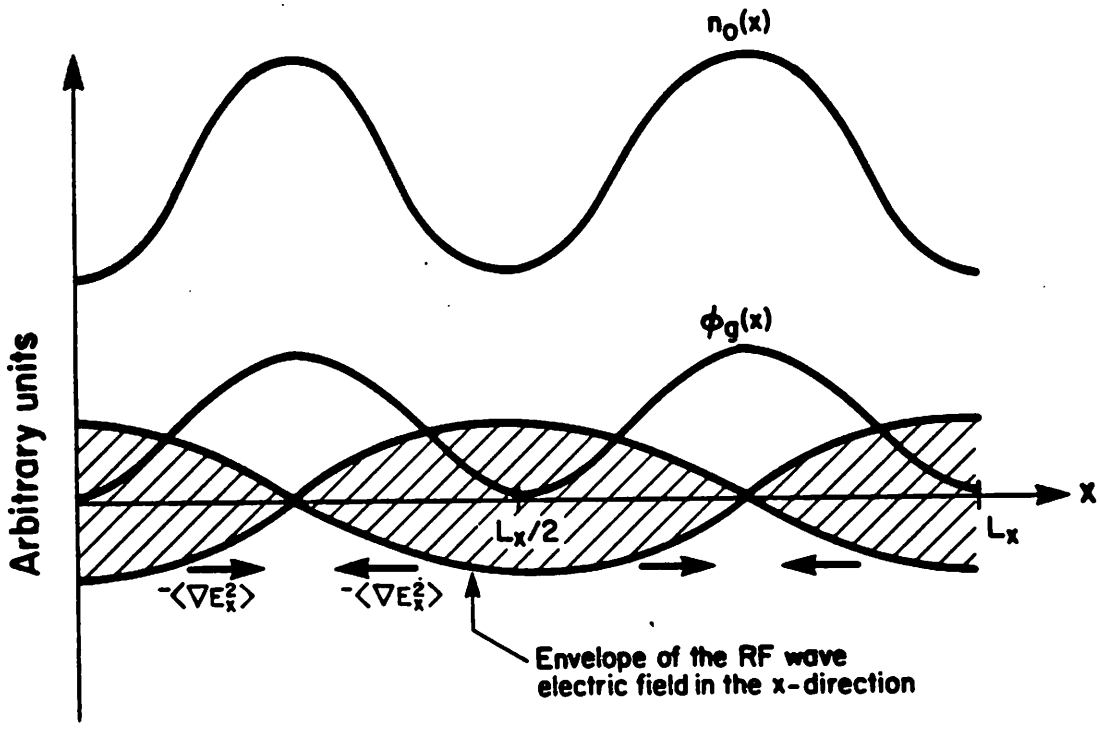

FIG. 3. Expected fast-timescale-averaged plasma density profile $n_0(x)$, gravitational potential profile $\phi_g(x)$, $(g(x) = -\nabla\phi_g(x))$, and x-directed RF wave electric field envelope in the presence of RF waves (i.e., in the modified equilibrium). Note that the negative gradient of the mean square electric field is directed antiparallel to $-\nabla\phi_g$ everywhere in the system.

system; however, Eq. (64) is more easily coded and is found to yield reasonably stationary small amplitude eigenmodes since $L_B^{-1} \ll L_n^{-1}$.

The presence of RF eigenmodes in our periodic system necessitates the use of two peaks in the density profile. When the longest-wavelength compressional Alfvén eigenmode is loaded in the system, the time-averaged gradient $\langle \nabla E_x^2 \rangle$ takes the form depicted in Fig. 3. Study of the stabilizing properties of such square-field gradients requires the density profile and gravitational field to be initialized so that the interchange-unstable regions of the plasma (∇n antiparallel to g) fall consistently in the regions where the magnitude of these gradients is maximum. The quantity ∇E_x^2 goes through two complete cycles in x; thus, as illustrated in Fig. 3, this condition is only satisfied when two density peaks are present, accompanied by two cycles of the gravity profile.

To complete the initialization procedure, a small perturbation is added to the particle positions and/or velocities. The perturbation parameters are chosen with the intention of exciting the interchange mode. The spatial dependence of the perturbation for most of our runs takes the form $\sin 2\pi m_x x/L_x \cos 2\pi m_y y/L_y$ where L_x and L_y are x- and y-lengths of the simulation system. In our simulations, the value of m_y is generally taken to be 1, with the interchange wavelength adjusted by varying L_y.

VIII. SIMULATION RESULTS

Results of the simulations fall naturally into three categories analogous to those described earlier. That is, we first verify properties of the time-independent equilibrium and next show the modified equilibrium (i.e., the equilibrium in the presence of the RF wave) behaves as expected. Properties of the low-frequency gravitational mode are also examined. Finally, the interactions between the RF wave and the interchange mode are discussed.

The most important characteristic of the time-independent equilibrium to verify is that it is indeed time-independent. When no RF eigenmode or interchange perturbation is loaded, we find this condition is well-satisfied. The criterion used in determining the equilibrium particle velocities (Sec. VII) guarantees that the particles feel no force initially. Small time-dependent disturbances appear in the electric field and $\hat{\mathbf{x}}$-directed current due to differencing errors in the finite-difference version of Eq. (5d), but these errors are found to be stable. No significant change is observed in the density, magnetic field, or gravitational current profiles through $\omega_{ci}t = 240$, the length of a typical run. It is of course also important that the density profile, velocity field, etc. vary with x as desired. This is also easily verified.

Behavior of the system in the presence of the RF eigenmode without the interchange mode is displayed in Figs. 4 and 5. The eigenmode excited is the lowest frequency eigenmode allowed in the system with antisymmetric wave magnetic field structure. Figure 4 shows plots versus time of various spatial Fourier components of the RF magnetic field and RF-induced ion current density in the x-direction. The modes of both plots exhibit near-sinusoidal time dependence as required. The observed presence of the shorter wavelength components is expected, since they appear also in the numerical calculation of the eigenmode as a consequence of the dependence of the time-independent equilibrium on x. The temporal behavior of E_y is also nearly sinusoidal; that of E_x is a bit messier (Fig. 5)

and becomes more so at larger wave amplitudes. We anticipate this to be acceptable, however, since the expected 90° phase shift between the two components is clearly present, and, more importantly, the required gradient $\langle \nabla E_x^2 \rangle$ is observed (Fig.5(b)) and persists in larger-amplitude waves.

The presence of the zero-frequency unstable gravitational mode described by Eqs. (19)–(21) has also been verified. When the entire ion particle population is initialized with a spatially-independent velocity perturbation in the x-direction, the density profile is observed to shift rigidly in the direction of the initial displacement. In effect, the density profile rolls down one side of the gravitational hill and back up the other side, as illustrated in Fig. 6. This instability has not caused problems in our simulations, since its growth rate is only of order the growth rate of the interchange instability. It is therefore not observed when not initialized in simulations started with a small but finite interchange perturbation.

Certain of the nonlinear characteristics of the RF mode have also been verified. The RF mode is initialized as an eigenmode only to linear order in wave field amplitudes in our simulations; thus, we expect the secular behavior outlined in Sec. IV to be operative

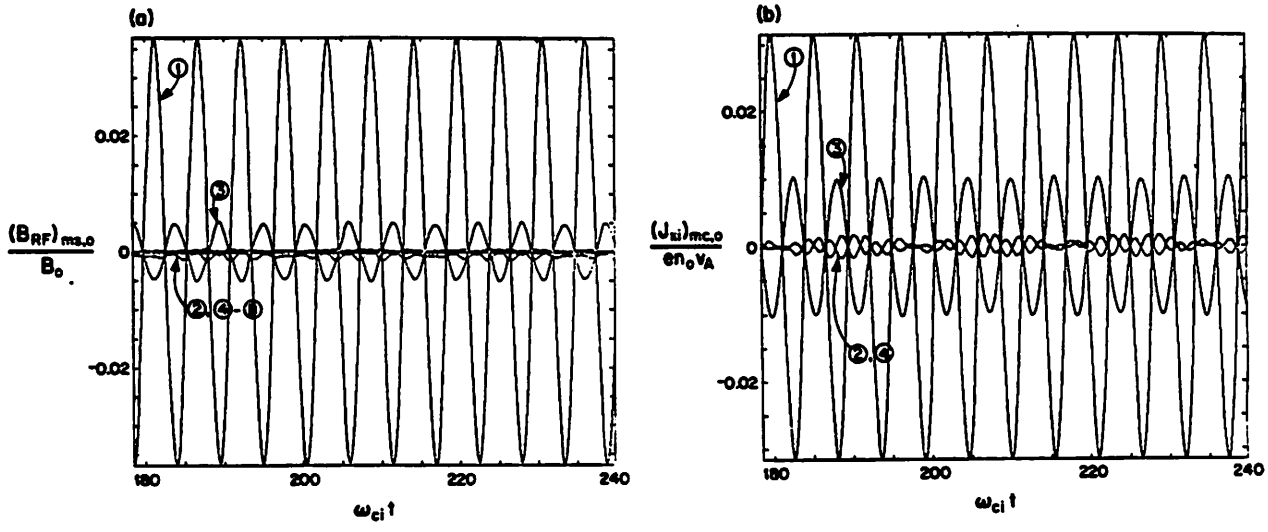

FIG. 4. (a) Spatial $\sin 2\pi mx/L_x$ Fourier modes of the simulation magnetic field versus time for $m = 1$ through 8 during a portion of a typical simulation run with initial parameters $B_{RF}/B_0 = 0.0375$, $n_l/n_0 = 0.5$, $N_i = 512$, $L_x = 32\Delta x$, $\omega_{ci}\Delta t = 0.03$, $v_A\Delta t/\Delta x = 0.219$, and $g_0 L_x/v_A^2 = 0.045$, where N_i is the number of ion simulation particles and Δx is the grid spacing in the x-direction. The expected eigenfrequency of the excited RF mode, $1.15\omega_{ci}$, agrees well with that observed in the simulation. The quantities ω_{ci} and v_A are evaluated at $x = 0$. (b) Spatial $\cos 2\pi mx/L_x$ Fourier modes of the x-directed ion current for $m = 1$ through 4 for the same run.

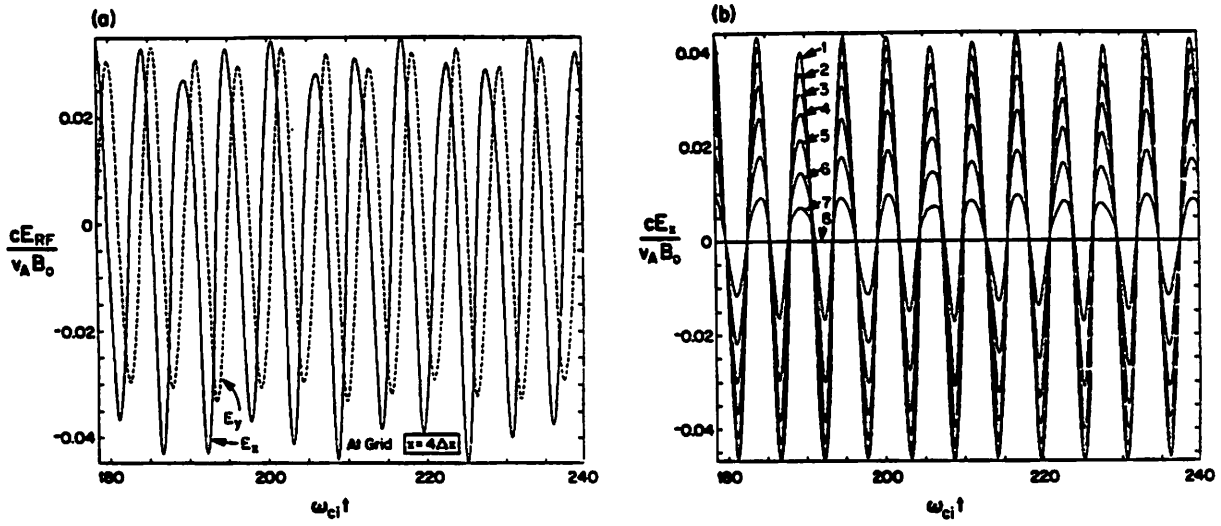

FIG. 5. (a) The x- and y-directed electric field components at x-grid-point 4 (i.e., at $x = 4\Delta x$) versus time for the run described in Fig. 4. (b) The x-directed electric field versus time at x-grid-points 1 through 8. The successive decrease in the wave amplitude at each grid-point implies the existence of the desired square electric field gradient.

at higher order. Figure 7 illustrates an example. The mode depicted (the $m_x = 2$, cosine component of the wave magnetic field) exhibits both the initial secular growth and d.c. offset predicted by Eq. (24). The d.c. offset is barely visible in the Figure, but is found to have the value -1.24×10^{-5}, in agreement with Eq. (25), when analyzed with the data post-processor ZED [28]. The initial secular growth is observed to be the linear portion of a relatively large sinusoidal wave envelope. The frequency ($\approx 2\omega_0$) also agrees well with the expected value (Eq. (24)).

Results consistent with theoretical expectations for the second-order current (Eqs. (27) through (29)) have also been obtained. Two simulations, one initiated with a strong RF wave ($B_1/B_0 = 15\%$) and one started without a wave were analyzed for changes to the destabilizing gravitational current. Diagnostics in the code allow the current to be studied when decomposed as

$$\frac{\langle (J_y)_{2s} \rangle}{en_0 v_A} = \frac{2k_0 c \langle B_{2c} \rangle}{4\pi e n_0 v_A} \tag{65a}$$

$$= \frac{\langle (J_{iy})_{2s} \rangle}{en_0 v_A} + \frac{c}{2B_0 n_0 v_A} \left(\langle n_{1c} E_{1s} \rangle + \langle n_{1s} E_{1c} \rangle \right) + \frac{c}{B_0 v_A} \langle E_{2s} \rangle - \frac{c}{2B_0^2 v_A} \left(\langle E_{1c} B_{1s} \rangle + \langle E_{1s} B_{1c} \rangle \right), \tag{65b}$$

where the subscripts c and s refer to the $\cos(2\pi n x/L_x)$ and $\sin(2\pi n x/L_x)$ components of the

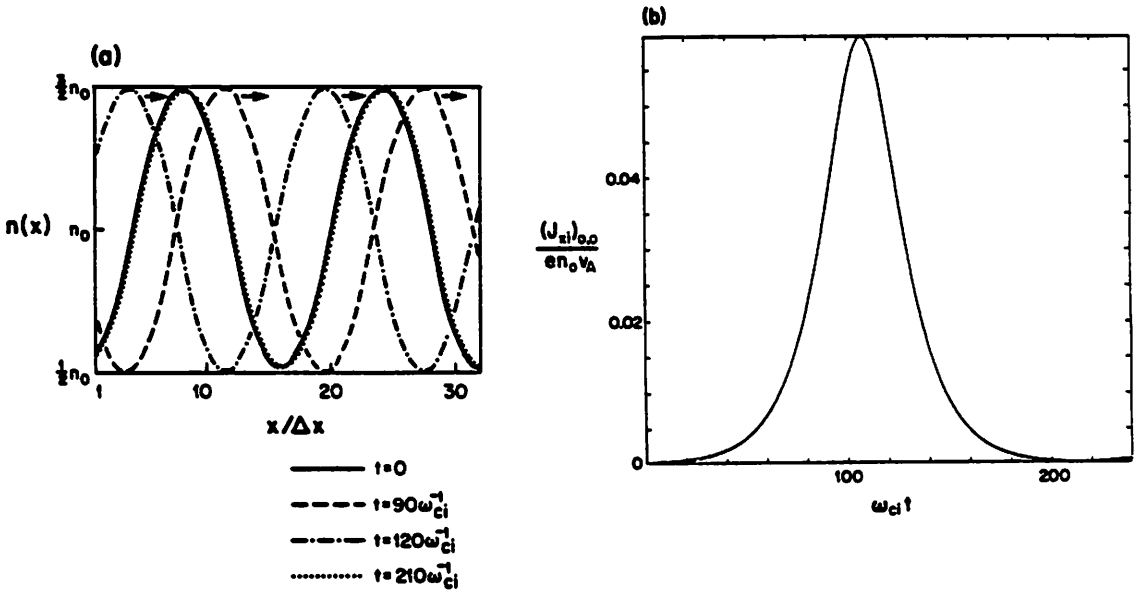

FIG. 6. (a) Snapshots of the density profile $n_0(x)$ at four times during a simulation initialized with a small spatially-independent velocity perturbation δu_x in the x-direction. The entire profile is observed to move to the right (indicated by the arrows) with little change in shape. At time $t = 210\omega_{ci}^{-1}$, the profile has moved almost exactly half a system length to the right to lie in coincidence with its initial configuration. (b) History of the x-component of the ion current shows the increase in the plasma velocity until the "bottom of the hill" is reached at time $t = 108\omega_{ci}^{-1}$. The velocity then decreases as the plasma rolls up the other side. In this run, $B_{RF} = 0$, $n_l/n_0 = 0.5$, $L_x/L_y = 0.167$, $N_i = 8192$, $L_x = 32\Delta x$, $L_y = 32\Delta y$, $\omega_{ci}\Delta t = 0.03$, $v_A\Delta t/\Delta x = 0.219$, and $g_0 L_x/v_A^2 = 0.045$. The perturbation was initialized with $m_x = 0$ and $\omega_{ci}\delta u_x/g_0 = 0.05$.

subscripted quantity where n is the numerical subscript. Since both g and ∇n_0 depend on x as $\sin[2\pi(2)x/L_x]$, the "2s" component of the $\hat{\mathbf{y}}$-directed current is the relevant current. The relation Eq. (65a) is required to approximate Ampère's Law as J is not computed directly by the code. In Eq. (65b), the first term represents the ion current, while the second and last two terms represent the $\langle n_1 u_{ey1}\rangle$ and $n_0\langle u_{ey2}\rangle$ components of the electron current, respectively.

Comparison of the two simulations reveals that the ion current is little changed ($< 5\%$) by the RF wave from its gravitational drift value $n_0 eg/\omega_{ci}$ (Fig. 8), and there is no change to the mean drift velocity of individual ion particles. We also find the electron current is dominated by the $\langle n_1 u_{ey1}\rangle$ component, as expected. We obtain $\langle n_1 u_{ey1}\rangle/n_0 v_A = -4.40 \times 10^{-3}$, while $\langle u_{ey2}\rangle/v_A = 6.89 \times 10^{-4}$.

Since the presumably important components $\langle u_{iy2}\rangle$ and $\langle u_{ey2}\rangle$ of the gravitational current are only weakly affected by the RF wave, it is not surprising that the stabilizing

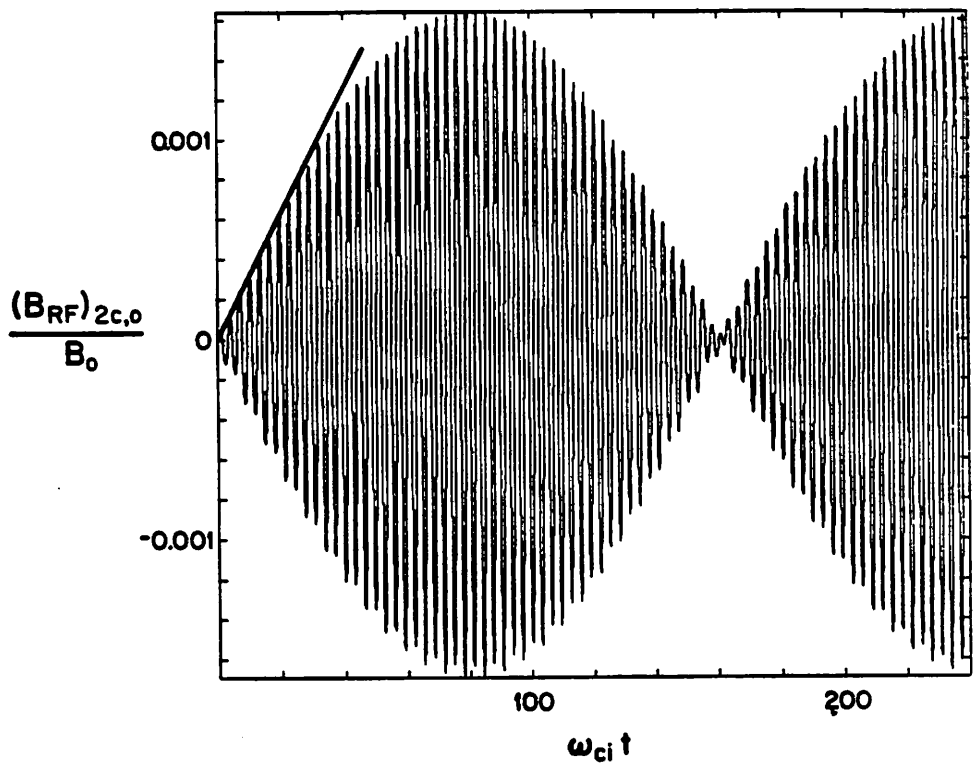

FIG. 7. Simulation example of the nonlinear secular behavior of the RF wave predicted by theory. Plotted is the $\cos 4\pi x/L_x$ Fourier component of the simulation magnetic field in a run initialized with $B_{RF}/B_0 = 0.01$, $n_i = n_0$, $N_i = 512$, $L_x = 32\Delta x$, $\omega_{ci}\Delta t = 0.03$, $v_A\Delta t/\Delta x = 0.155$, and $g_0 = 0$. The initial secular growth rate, defined by the slope of the slanted line, is found to agree with theory. The secular behavior at the beginning of the simulation is a portion of what appears to be a two-frequency beating phenomenon.

properties exhibited by the wave are modest at best when the interchange mode is excited. Figures 9(a)–(c) show the motion typical of selected ion-particles as the instability evolves in the absence of the RF wave. The displacement of the ions parallel to the $\pm\hat{y}$-axis is due to the gravitational drift and occurs most strongly in regions of maximum $|\nabla n_0|$ and $|g|$, as expected. Displacement in the $\pm\hat{x}$-direction is due to the interchange instability. As is the case in most of the runs, the longest wavelength ($kL_y = 2\pi$) was the one initially excited. This allows fewer grids to be used in the y-direction, fewer particles are then needed, and less computer time is thus required. Figures 9(d)–(f) show the effect of a large RF wave in an otherwise identical run. The compression and rarefaction of the ions due to the RF wave is clearly seen in some of the snapshots, and, as indicated earlier, the mean gravitational drift of the ions appears to be unaffected. Additional short-wavelength

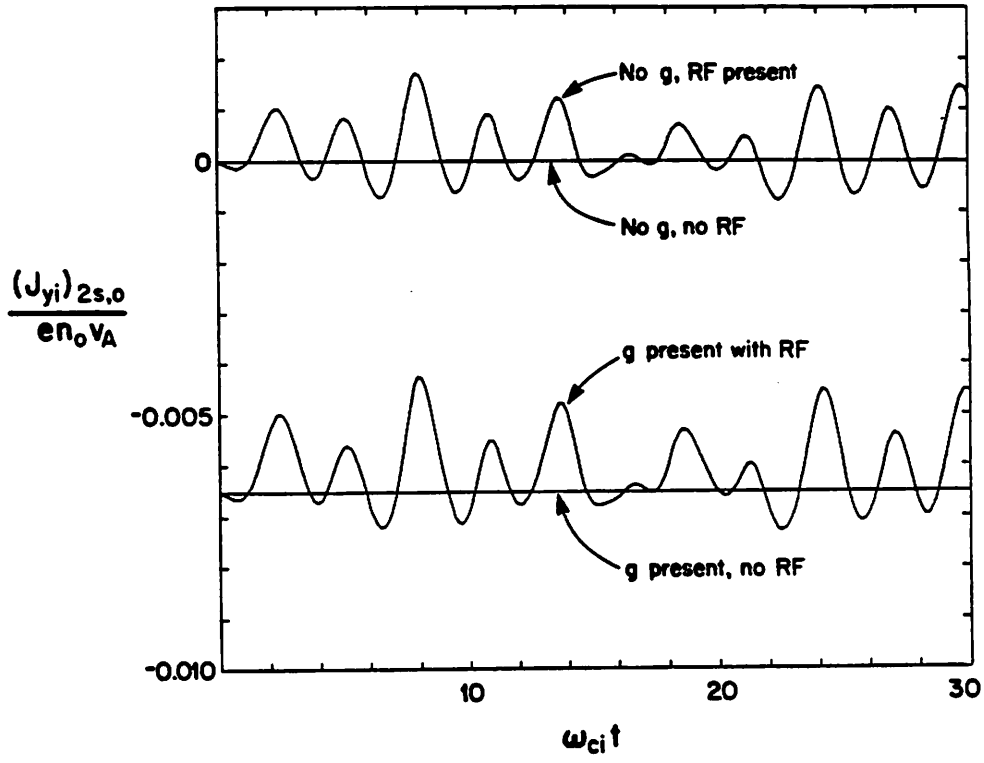

FIG. 8. The $\sin 4\pi x/L_x$ Fourier component of the y-directed ion current versus time for a portion of four simulation runs initialized with $n_i/n_0 = 0.5$, $N_i = 512$, $L_x = 32\Delta x$, $\omega_{ci}\Delta t = 0.03$, and $v_A\Delta t/\Delta x = 0.219$. This component of the ion current includes the ion gravitational current and corresponding RF modifications when gravity and RF, respectively, are present. In the runs in which gravity is present, $g_0L_x/v_A^2 = 0.045$; in the runs with RF is present, $B_{RF}/B_0 = 0.15$. The ion current observed for the g-present, no-RF case is found to agree with the theoretically expected value. Only small shifts in the time-averaged ion currents ($< 5\%$) are observed when RF is present.

structure in the x-direction is also visible, due probably to a different instability which becomes worse as L_x/L_y is increased, as described below. Also, the amplitude of the interchange perturbation is observed to be smaller owing to the slightly reduced growth rate (Fig. 10) produced by the presence of the RF wave. This example is in fact the case in which the most stabilization is obtained, and is shown to illustrate the extreme case. Other simulations exhibited significantly less change. In simulations in which L_x/L_y was small, except for the compressional motion of the plasma due to the RF wave, no effect whatever is observed.

There is, on the other hand, a substantial effect of the interchange mode on the RF

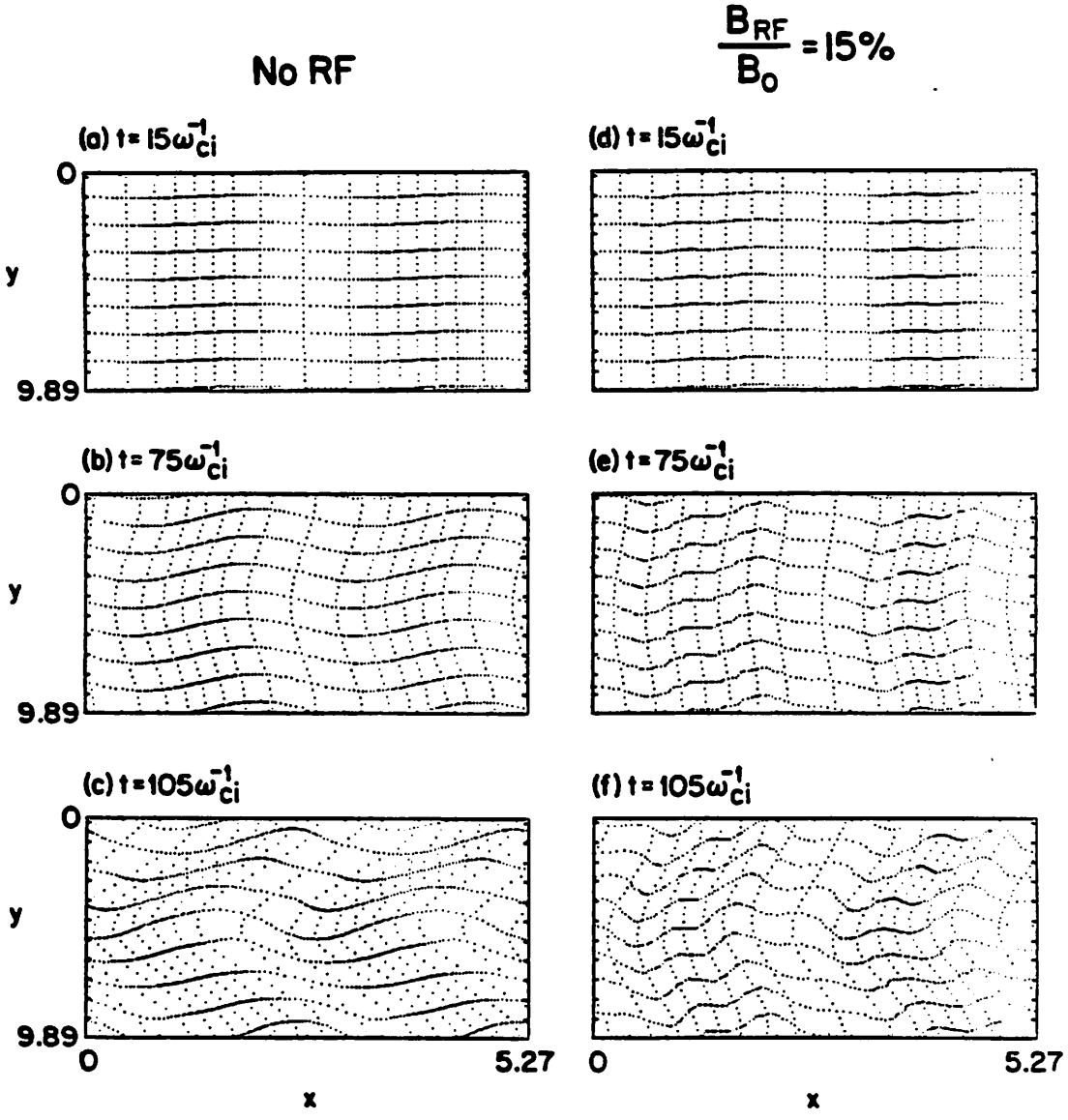

FIG. 9. Snapshots of *selected* ion simulation particles at various times for two simulations initialized with an interchange-like perturbation. Each "box" outlined by particles is actually filled with simulation particles initially arranged on the rectangular lattice suggested by the placement of the illustrated particles on the box edges. Plots (a) through (c) are snapshots from a run initialized without RF. The RF field was initialized with amplitude $B_{RF}/B_0 = 0.15$ in the run from which snapshots (d) through (f) were taken. Initially in both runs, $n_l/n_0 = 0.5$, $L_x/L_y = 0.533$, $N_i = 4096$, $L_x = 32\Delta x$, $L_y = 16\Delta y$, $\omega_{ci}\Delta t = 0.03$, $v_A\Delta t/\Delta x = 0.182$, and $g_0 L_x/v_A^2 = 0.054$. The interchange perturbation was excited with $m_y = 1$ and $\omega_{ci}\delta u_x/g_0 = 0.05$.

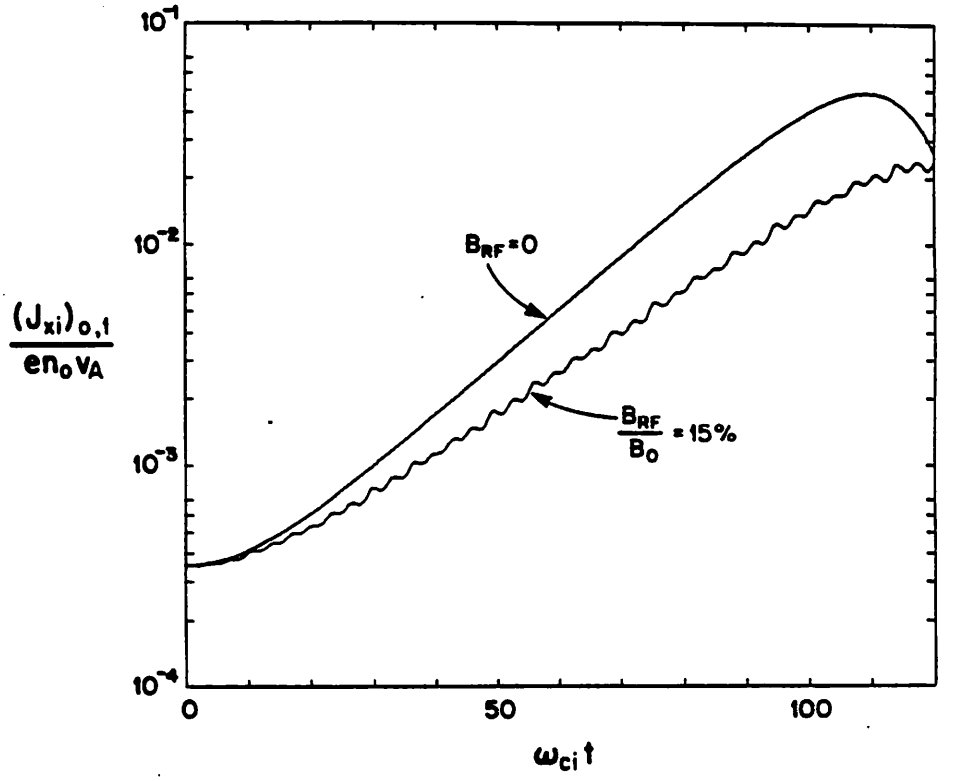

FIG. 10. The $m_x = 1$ component of the x-directed ion current versus time for the two simulations illustrated in Fig. 9. Both runs show clean linear growth with a slight reduction in the rate of growth observed in the simulation in which RF is present.

wave, as suggested by Similon and Kaufman [19]. Figure 11 illustrates the evidence. When the interchange is not excited, the RF wave amplitude is observed to maintain a constant amplitude as a function of time (Fig. 11(a)). In contrast, when the same system is initialized with an interchange perturbation, the RF field strength decreases dramatically as the interchange mode saturates (Fig. 11(b)).

The negligible-to-modest stabilizing effect of the RF wave on the interchange mode was the general rule over the parameter space we searched by means of a number of computer runs. The results of the parameter search are diagrammed in Figs. 12 and 13. In Fig. 12, the wavelength of the interchange mode was kept fixed by fixing the system length in its propagation direction L_y while allowing the equilibrium density scale length to change by varying L_x. The RF eigenmode frequency also varied from run to run, as indicated, since it depends on the system length in its propagation direction. Similarly, the growth rates in the absence of RF scale well with the theoretically expected $L_x^{-1/2} \sim L_n^{-1/2}$. The largest stabilizing effect occurred for $kL_n \sim L_x/L_y = 0.533$ when the growth rate was reduced by

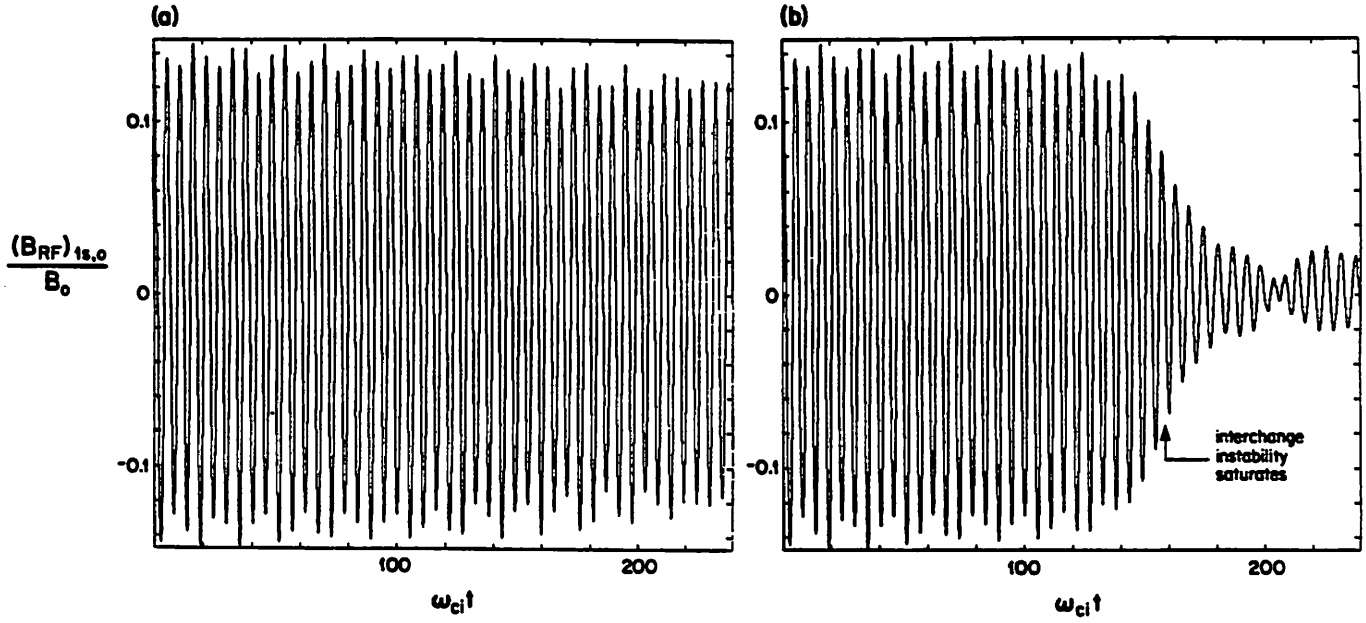

FIG. 11. Comparison of the wave magnetic field $\sin 2\pi x/L_x$ component in simulations in which the interchange mode (a) was not excited, and (b) was excited with saturation occurring at $t = 158\omega_{ci}^{-1}$. In these runs, initially, $B_{RF}/B_0 = 0.15$, $n_i/n_0 = 0.5$, $L_x = 32\Delta x$, $\omega_{ci}\Delta t = 0.03$, $v_A\Delta t/\Delta x = 0.219$, and $g_0 L_x/v_A^2 = 0.045$. The run in which the interchange mode was not excited was run in one dimension with $N_i = 512$. When the interchange mode was present, two dimensions were required with $L_x/L_y = 0.167$, $N_i = 8192$, and $L_y = 32\Delta y$. The interchange mode was excited with perturbation $\delta u_x(x) = 0.05\, mcg(x)/eB_0(x)$.

only 17% when $B_{RF}/B_0 = 15\%$, which would correspond to a tremendous field in an actual device. A slight destabilizing effect is observed for $L_x/L_y \gtrsim 0.8$.

When the density scale length, RF eigenfrequency, and theoretical natural growth rate are held constant by fixing L_x, while the interchange wavelength is allowed to vary, we observe the growth rates plotted in Fig. 13. The RF frequency was purposely chosen close to the ion-cyclotron frequency ($\omega_0 = 0.96\omega_{ci}$), since this is where the most dramatic effects would be expected if the cyclotron resonance plays a significant role. No such effect is observed however; instead, we again find only relatively weak stabilizing ($L_x/L_y \lesssim 0.9$) or weak destabilizing effects ($L_x/L_y \gtrsim 0.9$) considering the magnitude of the RF field employed ($B_{RF}/B_0 = 0.15$).

Three additional runs ($B_{RF}/B_0 = 0.0375$, 0.0750, and 0.1125) were made to determine the dependence of the stabilizing effect on the RF wave field strength for the case $L_x/L_y = 0.533$ illustrated in Fig. 13. The reduction in the interchange growth rate is seen to depend quadratically on the RF wave amplitude (Fig. 14) with the largest percentage reduction, ($-\Delta\gamma/\gamma = 23\%$), occurring for $B_{RF} = 0.15$. The quadratic dependence would be expected if the effective gravity driving the instability is reduced by a force scaling as the square of

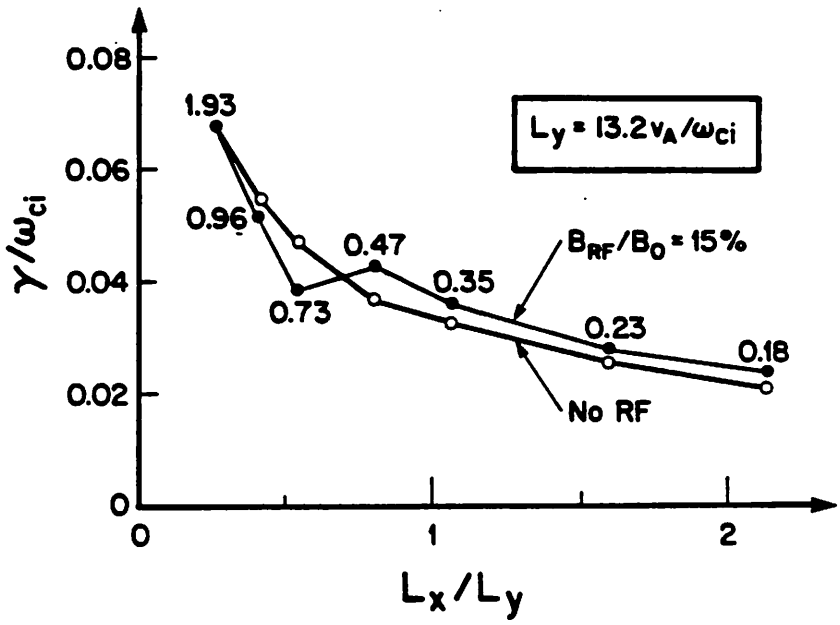

FIG. 12. Interchange mode growth rates for several simulations for which the system length in the y-direction is held fixed at $L_y = 13.2 v_A/\omega_{ci}$. Simulations are run in both the presence and absence of RF. The observed frequencies of the excited RF eigenmodes, indicated in units of ω_{ci} next to appropriate data points, were found to be within $0.01\omega_{ci}$ of their expected values. The initial parameters, $n_i/n_0 = 0.5$, $N_i = 4096$, $L_x/\Delta x = 32$, $L_y/\Delta y = 16$, $\omega_{ci}\Delta t = 0.03$, and $g_0 L_x/v_A^2 = 0.054$ are common to all runs. The interchange mode was excited with perturbation $\omega_{ci}\delta u_x/g_0 = 0.05$ for $m_y = 1$.

the RF wave amplitude.

A small set of runs with these parameters was also conducted for an RF standing wave initialized so that ∇E_x^2 was directed antiparallel rather than parallel to g(x) everywhere in the system. From the relative spatial phases described in Eqs. (22a) and (22e), it is clear that this requires ∇B_{RF}^2 to be pointing parallel to g. A different eigenmode with somewhat lower theoretical frequency $\omega_{RF} \approx 0.74$ is required to produce this field structure. With $B_{RF}/B_0 = 0.15$, the effect is again found to be stabilizing, producing a growth rate reduction of 15%, suggesting either that the sign of the electric field gradient, or even the gradient itself is not important in the stabilizing process, or that the magnetic field gradient ∇B_{RF}^2 also plays a role. The system length in the x-direction L_x was shortened somewhat ($L_x/L_y = 0.415$) for additional tests, raising the eigenfrequency of the RF mode back to $\omega_{RF} = 0.96\omega_{ci}$. The interchange growth rate was reduced by approximately 11% in the presence of RF ($B_{RF}/B_0 = 15\%$) for this case, and rough quadratic dependence of the reduction on the RF field amplitude was again observed.

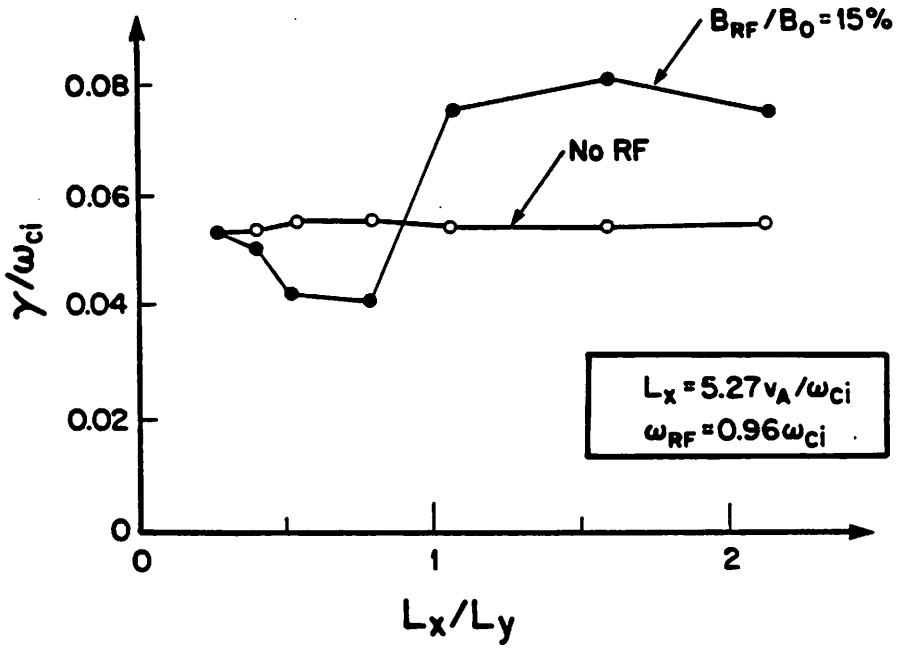

FIG. 13. Interchange mode growth rates in both the presence and absence of RF for several simulations in which the system length in the x-direction is held fixed at $L_x = 5.27 v_A/\omega_{ci}$. The initial parameters and interchange mode excitation are the same as described in Fig. 12. The two data points at $L_x/L_y = 0.4$ are common to this figure and Fig. 12. Detail of the simulations yielding the data points at $L_x/L_y = 0.533$ are illustrated in Figs. 9 and 10; growth rates for intermediate RF-field strengths for this set of parameters are shown in Fig. 14.

Finally, attempts to examine the stabilizing effects of RF on short-wavelength interchange modes ($L_x/L_y \gtrsim 2$) have been frustrated by the appearance of additional short-wavelength modes. These modes are apparently nonlinearly generated, since they only appear when the RF wave is present or when the interchange mode has saturated. Neither the identity of these modes nor the method by which they are generated is understood at present. It is also not clear whether these modes are physical or numerical in nature. They are not easily studied either by theoretical means, since they are nonlinearly generated, or by simulation, since they tend to congregate at the shortest available wavelengths of the system and are therefore poorly resolved. The presence of these modes also makes impossible our study of the interchange instability in this regime. As shown in Fig. 15, the short-wavelength modes appear before the interchange instability can be seen. The effect of the modes is to scatter ions from their regular pattern after which the ion fluid can no longer be regarded as cold. The simulation often terminates abnormally shortly after the

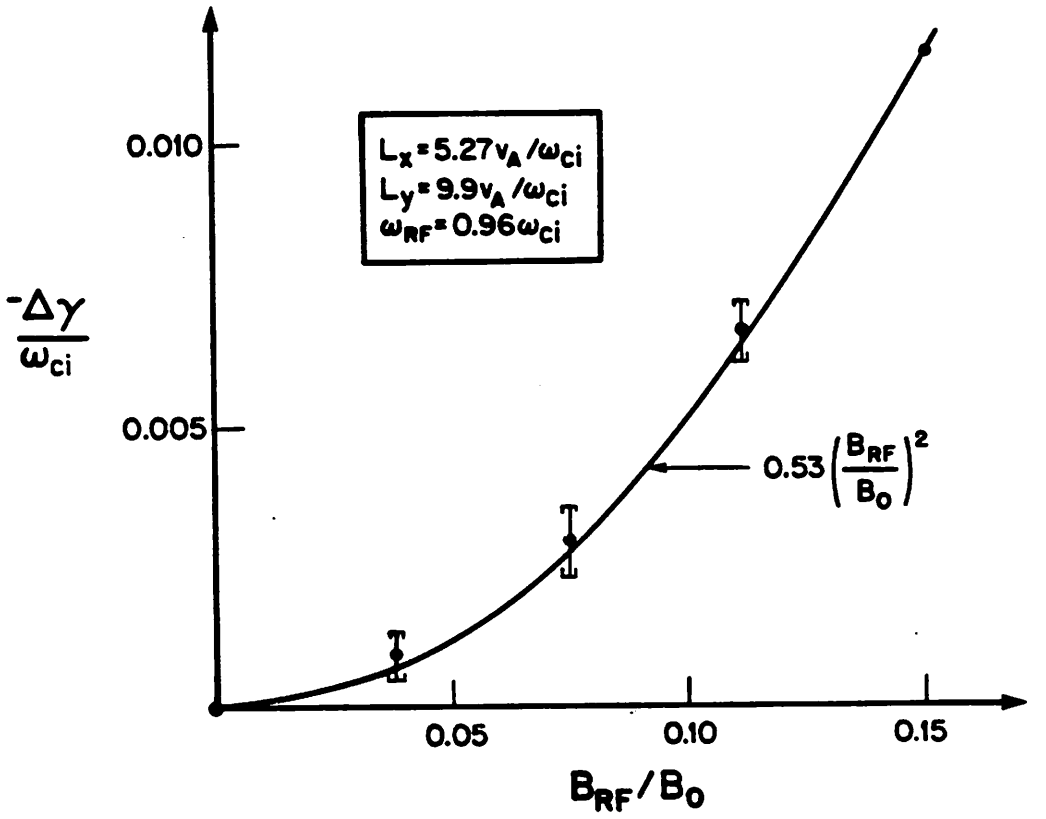

FIG. 14. Reduction in interchange growth rate $(-\Delta\gamma)$ for five runs with differing RF wave field strengths. The data points at $B_{RF}/B_0 = 0\%$ and 15% also appear in Fig. 13 $(L_x/L_y = 0.533)$. The data obtained are consistent with a square scaling law; the function $-\Delta\gamma/\omega_{ci} = 0.53(B_{RF}/B_0)^2$ is plotted for comparison.

regular pattern is lost as regions of low- or zero-density are generated.

IX. COMPARISON OF SIMULATIONS WITH EIKONAL THEORY

Direct comparison of the theory of Sec. VI to the simulation data is problematic. The simulations address low mode-number nonlocal interchange stability, and the RF and equilibrium gradients are comparable. Extension of analytical theory to low-mode number nonlocal theory for the interchange mode and the RF pump wave is nontrivial (see Refs. 18 and 26). In the low mode number limit, there is no reason to expect $\delta\mathbf{f}_{sb}$ to contribute negligibly to interchange stability. Furthermore, if we allow $\mathbf{k}\cdot\mathbf{B}_0 \neq 0$ for the pump wave and the sidebands, the sideband coupling might be substantially enhanced [15,18–20,26,27], particularly if the sidebands are normal modes for which $\det \mathbf{D}(k_\parallel, k_\perp, \omega_\pm) \to 0$ [15,20,27].

Nevertheless, some qualitative statement bearing on the simulation results can be made

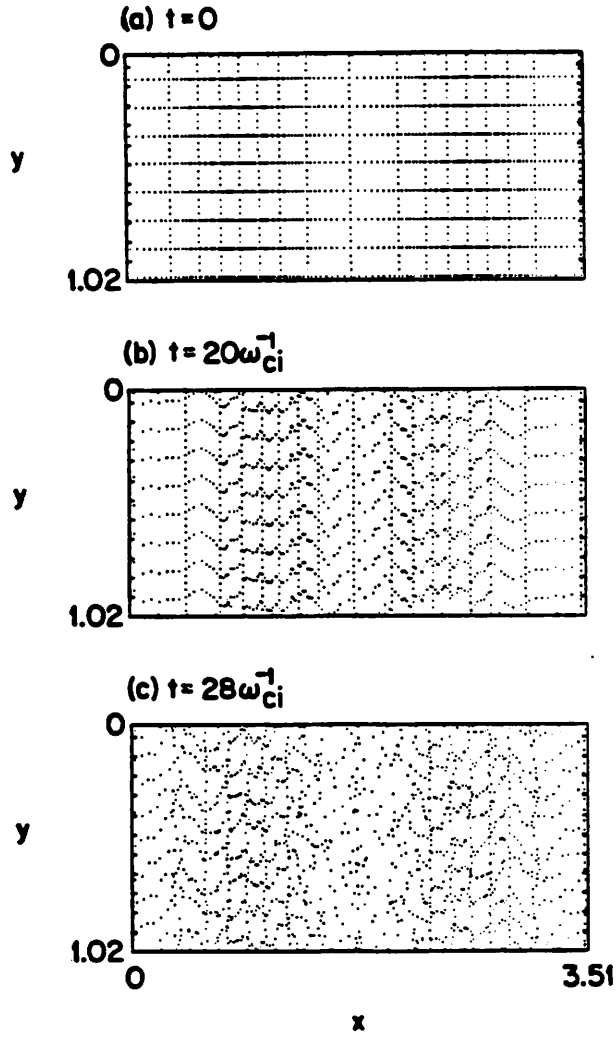

FIG. 15. Snapshots of selected particles in an run in which an unidentified nonlinear instability occurs. The instability typically appears at larger values of L_x/L_y and is characterized by short-wavelength structure in the y-directed particle drifts (b), followed by a breakup of the regular particle grid pattern (c). The breakup usually occurs first in the low-density regions and generally exhibits short-wavelength structure in both the x- and y-directions. This run was initialized with $B_{RF}/B_0 = 0.15$, $n_l/n_0 = 0.5$, $N_i = 4096$, $L_x = 32\Delta x$, $L_y = 16\Delta y$, $\omega_{ci}\Delta t = 0.016$, $v_A\Delta t/\Delta x = 0.146$, $g_0 L_x/v_A^2 = 0.022$. Displayed spatial dimensions are in units of v_A/ω_{ci}.

based on Eqs. (43) and (60). For $|B_x(\omega_0)/B_0|^2 \ll 1$ there must be substantial steepening of the RF amplitude gradient if the compressional Alfvén wave is to have a significant influence on interchange stability, at which point the RF ponderomotive force will have a large effect on the plasma equilibrium. In our simulations, the RF amplitudes satisfied $|B_x(\omega_0)/B_0| \leq 0.15$ and the ratio of the RF magnetic field gradient to the equilibrium magnetic field gradient was approximately 25. With these parameters, Eqs. (43) and (60) suggest a reduction in growth rate approximately equal to 30% for the maximum RF amplitude used, which is in surprisingly good agreement with the 25% reduction observed in the simulations. Furthermore, in the simulations stabilization increased with increasing RF gradient, was proportional to $|B_x(\omega_0)|^2$, and was independent of the sign of $\omega_0 - \omega_{ci}$. All of these observations agree with our analytical findings.

The good quantitative agreement of the theory with the simulations is perhaps fortuitous. When the gradient of the RF electric-field amplitude was directed parallel to the density gradient in the simulations so that the ponderomotive force was directed parallel to the gravity, the RF should have further destabilized the interchange modes according to the eikonal theory. Instead, the simulations indicated a 10–15% reduction in the interchange growth rate for $|B_x(\omega_0)/B_0| = 0.15$, i.e., approximately half of the reduction obtained when the ponderomotive force was directed opposite to the gravity. We suspect that these simulation observations may have been the result of finite contributions from $\delta \mathbf{f}_{sb}$ proportional to $(\partial n^{(0)}/\partial x)^2 |\tilde{E}_y(\omega_0)|^2$ that were independent of the RF gradient, always stabilizing, and comparable to or greater than those from $\delta \mathbf{f}_p$ in the limit that $|\mathbf{k}|$, $\nabla \ln |\mathbf{E}(\omega_o)|$, and $\nabla \ln n^{(0)}$ were all comparable. A concurring estimate of $\delta \mathbf{f}_{sb}$ can be inferred from the eikonal calculation of sideband coupling of magnetosonic waves and interchange modes presented in [15,20,27].

X. FUTURE DIRECTIONS

We have attempted in this study to examine some of the more interesting parameter regimes in order to obtain a preliminary understanding of the influence of RF waves on interchange modes. It was not our intention at this point in the study to make a complete search of all potentially stabilizing situations possible within the current version of the simulation model. Thus several other interesting possiblities still remain to be explored.

Traveling instead of standing waves may be expected to affect interchange stability because of gradients in the wave amplitude caused by the variation of the plasma density with x. This is especially true for short-wavelength RF waves ($kL_n \gg 1$), which in general have not been examined in simulations performed for this study. This regime involves finer resolution in the x-direction and therefore requires more computer time.

RF waves propagating partially or entirely in the y-direction may have some stabilizing effect. It may also be possible to include artificially characteristics of a finite-$k_\parallel$ RF wave in the field equations [29]. Both of these cases require improvements to the simulation algorithm.

The electrostatic ion-cyclotron wave could be used as the RF wave. This type of wave requires a finite electron temperature, a feature which exists in the code, but was not used

in this study. Ion-Bernstein modes are also a possibility, but would require many more ion-particles than is feasible at present.

Finally, the parameter search could be broadened. In this study, we examined modifications to the interchange growth rate produced directly by changes in the RF field strength and indirectly by changes to ω_0/ω_{ci} and kL_n through changes in L_x and L_y. The effects caused by variations to other parameters such as g_0 and L_n (through the ratio n_l/n_0) remains to be investigated.

XI. SUMMARY

The stabilization properties of a finite-amplitude compressional Alfvén eigenmode on the interchange mode have been studied by means of a 2-d quasineutral hybrid simulation code. The Alfvén eigenmode plays the role of an antenna-generated RF wave in a real mirror plasma. It is excited so as to propagate perpendicular to $\mathbf{B}_0$ with frequency of order the ion-cyclotron frequency and wavenumber k_0 of order the inverse density scale length.

Stabilizing effects in this system have also been studied theoretically. Fluid equations descriptive of the simulation system have been shown to conserve energy and magnetic flux. It is also demonstrated that the magnetic field is carried along with the electron fluid in this model.

Several properties of the excited RF wave have been derived from these equations. We find that the linear RF wave equation supports an unstable zero-frequency gravitational mode in addition to the expected compressional Alfvén modes. Both type of modes have been observed in simulation with properties agreeing with theory. A nonlinear analysis of the RF wave leads to the conclusion that the destabilizing mean relative drift between the electrons and ions is not affected by the RF wave. Instead, an electron RF-oscillation current appears whose impact on interchange stability is unclear. Similar effects on these currents and drifts are observed in simulation.

Theoretical methods are also applied to the system equations when an interchange mode is present. The usual interchange mode dispersion relation is recovered in the absence of an RF wave. For the considerably more complicated finite-RF-wave case, we present an eikonal theory of the effects of RF on interchange stability. Our analytical calculation concludes that the ponderomotive forces summed over species dominate sideband coupling in the high mode number limit. In the presence of the perpendicularly-propagating compressional Alfvén RF wave in the eikonal limit, it is found that the reduction in the interchange growth rate is proportional to the ratio $\nabla B_{RF}^2/\nabla B_0^2$. The growth rate reduction thus scales quadratically with RF wave amplitude and is devoid of any ion-cyclotron resonance effects.

Simulations of the interchange mode in the presence of an RF wave chosen so that ∇E_x^2 is oriented parallel, ∇B_{RF}^2 antiparallel, to g(x) show only small stabilizing effects for the RF amplitudes employed ($B_{RF}/B_0 = 15\%$). The reduction in the interchange growth rate is seen to scale as the square of the RF field amplitude and shows no change in behavior as the RF frequency crosses the ion-cyclotron resonance, consistent with the eikonal theory. Additionally, the modest degree of stabilization observed is of the same order predicted by the theory. Good quantitative agreement is in fact obtained, but is probably fortuitous,

as is illustrated by simulations with directions of ∇E_x^2 and ∇B_{RF}^2 reversed. We find the effect is still stabilizing for this case, but is somewhat reduced. This is not consistent with the eikonal theory, which predicts a destabilizing influence. The percentage change in the growth rate is comparable however, and its observed magnitude suggests the presence of an additional gradient-independent stabilizing effect negligible in the eikonal limit.

We note that the ponderomotive and sideband coupling effects evidently do not exactly cancel one another in influencing interchange stability in our slab simulations at low mode number. This does not necessarily contradict recent calculations by D'Ippolito and Myra who find an exact cancellation of nonlinear effects in the volume of a cylindrical plasma (only surface terms are left) for $m = 1$ modes that are exactly rigid.

Slight destabilizing effects are observed for $kL_n \gtrsim 0.9$ with unidentified instabilities occurring for $kL_n \gtrsim 2$–3. We suspect that all the simulations with $kL_n \geq O(1)$ may be spoiled to some degree by numerical problems, as yet not understood by us. Finally, while the presence of RF only mildly affects the interchange growth rate, the reverse interaction, the effect of the interchange mode on the RF wave amplitude, is observed to be substantial, damping the RF wave significantly as the interchange mode saturates.

ACKNOWLEDGMENTS

The authors have benefited greatly from several conversations with Dr. J. A. Byers on several of the topics contained in this work. We are also grateful for the numerous valuable suggestions provided by Prof. C. K. Birdsall, Dr. M. J. Gerver, Dr. H. Hojo, Prof. A. N. Kaufman, Dr. T. D. Rognlien, and Dr. P. L. Similon. Computational facilities were provided by the National Magnetic Fusion Energy Computer Center. This work was supported by U. S. Department of Energy Contract No. DE-AT03-76ET53064 and U. S. Department of Energy Contract No. W-7405-ENG-48 through the Lawrence Livermore National Laboratory.

APPENDIX A. EXISTENCE OF AN UNSTABLE GRAVITATIONAL MODE

The 1-d wave equation Eq. (19) may be converted to an ordinary differential eigenvalue equation by assuming solutions of the form $u_{x1}(x,t)B_0(x) = \psi(x)\exp(-i\omega t)$. The equation obtained,

$$\frac{d^2\psi}{dx^2} + \left[\frac{1}{L_B}\left(\frac{1}{L_B} - \frac{1}{L_n}\right) + \frac{\omega^2}{v_A^2}\right]\psi = 0, \tag{A1}$$

is of the Sturm-Liouville form

$$\frac{d}{dx}\left(p\frac{d\psi}{dx}\right) + (q + \lambda r)\psi = 0, \tag{A2}$$

where $p = 1$, $q = L_B^{-1}\left(L_B^{-1} - L_n^{-1}\right)$, $r = 1/v_A^2$, and the eigenvalue $\lambda = \omega^2$.

Sturm-Liouville theory must be modified in our case to accomodate periodic boundary conditions. A number of properties are easily derived:

(a) The operator $L \equiv (d/dx)(p\,d/dx) + q$ is Hermitian if $p(0) = p(L_x)$; i.e.,

$$\int dx\,\psi^* L\psi = \left[\psi^* p\frac{d\psi}{dx} - \psi p\frac{d\psi^*}{dx}\right]_0^{L_x} + \int dx\,(L\psi^*)\,\psi$$
$$= \int dx\,(L\psi^*)\,\psi \quad \text{if} \quad p(0) = p(L_x). \tag{A3}$$

(b) The eigenvalues $\{\lambda_n\}$ are then real, since

$$-\lambda_n \int dx\,\psi_n^* r\psi_n = \int dx\,\psi_n^* L\psi_n = \int dx\,(L\psi_n^*)\,\psi_n = -\lambda_n^* \int dx\,\psi_n^* r\psi_n, \tag{A4}$$

implies $\lambda_n = \lambda_n^*$.

(c) The eigenfunctions $\{\psi_n\}$ may be chosen to be real:

$$L\left(\frac{\psi_n + \psi_n^*}{2}\right) = -\frac{r\lambda_n\psi_n}{2} - \frac{r\lambda_n^*\psi_n^*}{2} = -r\lambda_n\left(\frac{\psi_n + \psi_n^*}{2}\right). \tag{A5}$$

(d) These real eigenfunctions are orthonormal in the sense:

$$\int dx\,\psi_n r\psi_m = \delta_{nm}, \tag{A6}$$

if the eigenfunctions $\{\psi_n\}$ are normalized so that $\int dx\,r\psi_n^2 = 1$, since

$$-\lambda_m \int dx\,\psi_n r\psi_m = \int dx\,\psi_n L\psi_m = \int dx\,\psi_m L\psi_n = -\lambda_n \int dx\,\psi_n r\psi_m, \tag{A6}$$

implies the integral is zero unless $\lambda_m = \lambda_n$. When $\lambda_m = \lambda_n$ for $m \neq n$, there normally exists a degenerate subspace of eigenfunctions for which an orthonormal basis may be chosen.

With these properties, consider the integral,

$$\int dx\,\psi^* L\psi = \int dx\,\psi\left(\frac{d}{dx}p\frac{d\psi}{dx} + q\psi\right) = -\int dx\left(p\left|\frac{d\psi}{dx}\right|^2 - q|\psi|^2\right). \tag{A7}$$

Assuming ψ is decomposable in terms of the eigenfunctions of L as

$$\psi = \sum_{n=0}^{\infty} a_n\psi_n, \tag{A8}$$

we find, using the orthogonality properties, that

$$\int dx\,r|\psi|^2 = \sum_n |a_n|^2, \tag{A9}$$

and

$$-\int dx\,\psi^* L\psi = \sum_n |a_n|^2\,\lambda_n \geq \sum_n |a_n|^2\,\lambda_0, \tag{A10}$$

for the lowest eigenvalue λ_0 of Eq. (A2). Thus the lowest eigenvalue must satisfy

$$\lambda_0 \leq \frac{\int dx \left(p \left| \frac{d\psi}{dx} \right|^2 - q|\psi|^2 \right)}{\int dx\, r|\psi|^2}. \tag{A11}$$

for all periodic functions ψ decomposable as indicated by Eq. (A8). For our equation (A1), the condition translates to

$$I[\psi] \equiv \frac{\int dx \left\{ \left| \frac{d\psi}{dx} \right|^2 - \frac{1}{L_B} \left(\frac{1}{L_B} - \frac{1}{L_n} \right) |\psi|^2 \right\}}{\int dx \frac{|\psi|^2}{v_A^2}} \geq \omega_{(0)}^2, \tag{A12}$$

where $\omega_{(0)}^2$ is the lowest eigenvalue of Eq. (A1).

This condition holds in particular for the presumably decomposable trial function $\psi(x) = \bar{\psi}$, independent of x. Since $\psi = u_{x1} B_0$ and B_0 is typically weak function of x, this function corresponds to a nearly incompressible, nearly rigid perturbation displacement in the x-direction. By continuing to assume B_0 is a weak function of x, we find

$$I[\bar{\psi}] \approx -\frac{\int dx \frac{1}{L_B} \left(\frac{1}{L_B} - \frac{1}{L_n} \right)}{\int \frac{dx}{v_A^2}} \approx \frac{\int dx \frac{B_0}{4\pi m n_0} \frac{dB_0}{dx} \frac{dn_0}{dx}}{\int dx\, n_0}, \tag{A13}$$

i.e., from Eq. (18),

$$I[\bar{\psi}] \approx \frac{\int dx\, g\, (dn_0/dx)}{\int dx\, n_0}. \tag{A14}$$

The numerator of this last quantity is always negative in our interchange-unstable equilibria, so the lowest eigenvalue, $\omega_{(0)}^2$, must be negative. There is therefore at least one unstable solution to Eq. (A1); furthermore, its growth rate γ may be expected to satisfy

$$\gamma^2 \equiv -\omega_{(0)}^2 \geq -\frac{\int dx\, g\, (dn_0/dx)}{\int dx\, n_0}. \tag{A15}$$

Thus γ scales as $(g/L_n)^{1/2}$, the growth rate of the short-wavelength interchange instability.

References

[1] J. R. Ferron, N. Hershkowitz, R. A. Breun, S. N. Golovato, and R. Goulding, "RF Stabilization of an Axisymmetric Mirror," Physical Review Letters **51**, 1955 (1983).

[2] G. Dimonte, B. M. Lamb, and G. J. Morales, "Ponderomotive Pseudopotential Near Gyroresonance," Physical Review Letters **48**, 1352 (1982).

[3] H. Akimune, I. Ikeda, T. Hirata, and F. Okamoto, "Dynamic Stabilization of Flute Instability," Journal of the Physical Society of Japan **50**, 2729 (1981).

[4]M. Inutake, K. Ishii, A. Itakura, I. Katanuma, T. Kawabe, Y. Kiwamoto, A. Mase, S. Miyoshi, T. Saito, K. Sawada, D. Tsubouchi, K. Yatsu, M. Aizawa, T. Kamimura, R. Itatani, and Y. Yasaka, "Studies on Improvement of Plasma Confinement in Axisymmetrized Tandem Mirror," in *Plasma Physics and Controlled Nuclear Fusion Research* (IAEA, Vienna 1983), Vol. I, p. 545.

[5]S.-I. Kishimoto, Y. Yamamoto, H. Akimune, and T. Suita, "Stabilization of Flute Instability by Means of High Frequency Field," Journal of the Physical Society of Japan **38**, 231 (1975).

[6]Y. Yamamoto, S.-I. Kishimoto, H. Akimune, and T. Suita, "Stabilization of Flute Instability by High Frequency Field," Journal of the Physical Society of Japan **39**, 795 (1975).

[7]G. Dimonte, B. M. Lamb, and G. J. Morales, "Effects of Nonadiabaticity on Applications of the Ponderomotive Force Near Gyroresonance," Plasma Physics **25**, 713 (1983).

[8]B. M. Lamb, G. Dimonte, and G. J. Morales, "Behavior of the Ponderomotive Effect Near Gyroresonance," Physics of Fluids **27**, 1401 (1984).

[9]J. R. Cary, "Relation of Fluid Drift to Oscillation Center Drift," Physics of Fluids **27**, 2193 (1984).

[10]B. I. Cohen and T. D. Rognlien, "Ponderomotive and Sideband Coupling Effects of Ion-Cyclotron Heating on Interchange Stability," Physics of Fluids **28**, 2793 (1985).

[11]D. A. D'Ippolito and J. R. Myra, "Quasilinear Theory of the Ponderomotive Force: Induced Stability and Transport in Axisymmetric Mirrors," Physics of Fluids **28**, 1895 (1985).

[12]N. C. Lee and G. K. Parks, "Ponderomotive Force in a Warm Two-Fluid Plasma," Physics of Fluids **26**, 724 (1983).

[13]G. Statham and D. terHaar, "Strong Turbulence of a Magnetized Plasma: II. The Ponderomotive Force," Plasma Physics **25**, 681 (1983).

[14]J. R. Cary and A. N. Kaufman, "Ponderomotive Force and Linear Susceptibility in Vlasov Plasma," Physical Review Letters **39**, 402 (1977).

[15]J. B. McBride, "Radio Frequency Stabilization of Electrostatic Interchange Modes," Physics of Fluids **27**, 324 (1984), and Erratum: N. A. Krall and J. B. McBride, Physics of Fluids **28**, 2022 (1985).

[16]V. Stefan and J. B. McBride, "Stabilization of Interchange Modes in Mirror Plasmas by Resonant Coupling to Ion-Cyclotron Sidebands," Physics of Fluids **28**, 3189 (1985).

[17]Ya. B. Faĭnberg and V. D. Shapiro, "Drift Instabilities of a Plasma Situated in a High-Frequency Electric Field," Soviet Physics JETP **25**, 189 (1967) [Russian Orig. Zh. Ehksp. Teor. Fiz. **52**, 293 (1967)].

[18]J. R. Myra and D. A. D'Ippolito, to appear in Nuclear Fusion, 1986.

[19]P. L. Similon and A. N. Kaufman, "Theory of Ponderomotive Stabilization of a Magnetically Confined Plasma," Physical Review Letters **53**, 1061 (1984).

[20]J. B. McBride and V. Stefan, "Scattering of Magnetosonic Waves off Interchange Modes in Mirror Plasmas," Physics of Fluids **29**, 1181 (1986).

[21]R. M. Pirsig, *Zen and the Art of Motorcycle Maintenance* (W. Morrow and Co., New York, 1974).

[22]N. F. Otani, "PEPSI: A 2 1/2-Dimensional Quasineutral Darwin Simulation Code," First and Second Quarter Progress Report on Plasma Theory and Simulation, January 1 to June 30, 1983, Electronics Research Laboratory, University of California, Berkeley, CA 94720.

[23]See, for example, J. T. Cushing, *Applied Analytical Mathematics for Physical Scientists* (Wiley, New York, 1975), Sec. 8.3.

[24]K. Sakai, S. Takeuchi, and M. Matsumoto, Yamanishi University, Japan, private communication, 1985.

[25]H. Abe, Kyoto University, Japan, private communication, 1985.

[26]J. R. Myra and D. A. D'Ippolito, "RF-Induced Stability and Transport in Axisymmetric Tandem Mirrors," Physical Review Letters **53**, 914 (1984).

[27]J. B. McBride, V. Stefan, and N. A. Krall, "Stabilization of Interchange Modes in Mirror Plasma Devices by Radio-Frequency Sideband Coupling," Physical Review Letters **54**, 42 (1985).

[28]N. F. Otani, "Availability of ZED Postprocessor on MFE-CRAY Computers" and "Generation of Data Files Compatible with the MFE-Cray Version ZED Postprocessor," First and Second Quarter Progress Report on Plasma Theory and Simulation, Jan. 1, 1982–June 30, 1982, Electronics Research Laboratory, University of California, Berkeley, CA 94720.

[29]P. L. Similon, private communication.